ZINC PHTHALOCYANINE-INCORPORATED MESOPOROUS SILICA NANOPARTICLES FOR PHOTODYNAMIC THERAPY OF CANCER

by

Hazal Öztürk Çulcu

B.S., in Biomedical Engineering, Kocaeli University, 2018

Submitted to the Institute of Biomedical Engineering
in partial fulfillment of the requirements
for the degree of
Master of Science
in
Biomedical Engineering

Boğaziçi University
2024

ZINC PHTHALOCYANINE-INCORPORATED MESOPOROUS SILICA NANOPARTICLES FOR PHOTODYNAMIC THERAPY OF CANCER

APPROVED BY:

Assist. Prof. Mustafa Kemal Ruhi .....
(Thesis Advisor)

Prof. Bora Garipcan .....

Assist. Prof. Melike Güney Akkurt .....

DATE OF APPROVAL: 16 August 2024

ACKNOWLEDGMENTS

My sincere gratitude to my advisor, Mustafa Kemal Ruhi, for his support and guidance throughout my thesis period. I would also like to thank my previous advisor, Murat Gülsoy, for his teachings and support.

I deeply appreciate the support and friendship of the Biophotonics Lab members, who have been an integral part of my journey. I want to express my special thanks to Dr. Burcu Güleryüz and Ayşe Işık for their invaluable approach and guidance. I would also like to thank my colleagues Sena Şişman and Tuğçe Mutlu, who supported and motivated me throughout this process.

I would also like to thank Prof. Bora Garipcan and the Biomaterial Lab and Cell Culture Lab members for their contributions and collaborations.

Lastly, I would like to thank my mother, Mehtap Öztürk, my family, and my dear friend, Nurşah Karaman Aksoy, for always supporting and loving me. And, of course, I am grateful to my dear husband, Çağrı Çulcu, for his extraordinary support and patience throughout this process.

ACADEMIC ETHICS AND INTEGRITY STATEMENT

I, Hazal Öztürk Çulcu, hereby certify that I am aware of the Academic Ethics and Integrity Policy issued by the Council of Higher Education (YÖK) and I fully acknowledge all the consequences due to its violation by plagiarism or any other way.

Name :

Signature:

Date:

ABSTRACT

ZINC PHTHALOCYANINE-INCORPORATED MESOPOROUS SILICA NANOPARTICLES FOR PHOTODYNAMIC THERAPY OF CANCER

Cancer is a common severe disease; many people suffer from it, and it shows a high mortality rate across the world. Traditional cancer treatments including chemotherapy, surgery, and radiotherapy have some significant drawbacks such as deprivation of targeting, complications from surgery. Photodynamic therapy (PDT) is a promising method for establishing novel cancer treatment modalities as it offers a selective targeting mechanism and uses nonionizing radiation. PDT requires nontoxic light-sensitive photochemical agents, which are called photosensitizers (PS), and they can be activated with light exposure, generating reactive oxygen species (ROS), which triggers cell death. However, PSs may have some limitations, such as low water solubility, aggregation, and bioavailability, which leads to insufficient accumulation of the therapeutic target. Therefore, nanoparticle-based drug delivery systems can enhance the targeting of such agents and release them with controllable photoactivity at predetermined locations, thus obtaining desired therapeutic effects with minimal adverse effects. In this study, the PDT potential of Zinc Phthalocyanine (ZnPc) incorporated Mesoporous silica nanoparticles (MSNs) was investigated on A-549 lung adenocarcinoma cell line by analyzing dark cytotoxicity, stability, cellular uptake, and light exposure assays. As a result, ZnPc-MSN demonstrated low dark toxicity, significant cellular uptake, and potent singlet oxygen generation upon the light exposure, demonstrating their potential as an effective PS. Further research will evaluate the surface modification of ZnPc-MSN to increase cellular uptake and augment the endosomal escape efficacy of in vivo experiments. Additionally, dual PS loading will be evaluated to increase the PDT effect.

Keywords: Cancer, Photodynamic Therapy, Zinc Phthalocyanine, Mesoporous Silica Nanoparticles

ÖZET

KANSERİN FOTODİNAMİK TERAPİSİ İÇİN ÇİNKO FTALOSİYANİN YÜKLÜ MEZOGÖZENEKLİ SİLİKA NANOPARTİKÜLLER

Kanser, dünya genelinde milyonları etkileyen ve yüksek ölüm oranlarına yol açan ciddi bir hastalıktır. Geleneksel tedavi yöntemleri olan kemoterapi, cerrahi ve radyoterapi, kanser hücrelerinin yanı sıra sağlıklı dokuları da etkileyerek önemli yan etkilere neden olur. Bu nedenle, hedefli ve yan etkileri daha az olan yeni tedavi yöntemleri araştırılmaktadır. Fotodinamik terapi (FDT), kanser tedavisinde umut veren bir yöntem olarak öne çıkmaktadır. FDT, ışığa duyarlı kimyasal ajanlar (fotosensitizanlar) ve iyonize olmayan ışık kullanılarak çalışır. Bu yöntemde, fotosensitizanlar kanser hücrelerine biriktirilir ve daha sonra belirli bir dalga boyundaki ışık ile aktive edilir. Aktive olan fotosensitizanlar, hücre içinde zararlı moleküller (reaktif oksijen türleri) oluşturarak kanser hücresini yok eder. Bu sayede, sağlıklı dokulara zarar vermeden sadece kanser hücreleri hedeflenir. Ancak, fotosensitizanların düşük suda çözünürlük, hücre içinde birikimde zorluk gibi bazı sınırlamaları bulunabilmektedir. Bu sorunu aşmak için fotosensitizanları nanopartiküllerle birleştirerek daha etkili hale getirilmeye çalışılmaktadır. Bu çalışmada, Çinko Ftalosiyanin (ZnPc) yüklü Mezogözenekli silika nanopartiküllerinin (MSN) fotodinamik terapötik potansiyeli, karanlık sitotoksisite, kararlılık, hücresel alım ve ışık maruziyeti analizleri ile A-549 akciğer adenokarsinomu hücre hattında araştırılmıştır. Sonuç olarak, ZnPc-MSN düşük karanlık toksisitesi, önemli hücresel alım ve ışıkta güçlü tekli oksijen üretimi göstererek etkili bir fotosensitizör olarak potansiyelini ortaya koymuştur. Gelecek araştırmalar, hücresel alımı artırmak ve in vivo deneylerin endosomal kaçış etkinliğini artırmak için MSN yüklü ZnPc'nin yüzey modifikasyonunu değerlendirecektir. Ek olarak, PDT etkisini artırmak için çift fotosensitizör yüklemesi dikkate alınacaktır.

Anahtar Sözcükler: Kanser, Fotodinamik Terapi, Çinko Ftalosiyanin, Mezogözenekli Silika Nanopartiküller

TABLE OF CONTENTS

ACKNOWLEDGMENTS iii
ACADEMIC ETHICS AND INTEGRITY STATEMENT iv
ABSTRACT v
ÖZET vi
LIST OF FIGURES ix
LIST OF SYMBOLS xii
LIST OF ABBREVIATIONS xiii
1. INTRODUCTION 1
1.1 Motivation and Objectives 2
2. BACKGROUND 3
2.1 Lung Cancer 3
2.2 Treatment of Lung Cancer 4
2.3 Photodynamic Therapy 6
2.4 Photosensitizers 9
2.5 Nanoparticles in Photodynamic Therapy 10
2.6 Zinc Phthalocyanine 12
2.7 Mesoporous Silica Nanoparticles 14
3. MATERIALS AND METHODS 17
3.1 Synthesis of Mesoporous Silica 17
3.2 Loading ZnPc into the MSN 18
3.3 Characterization of Nanoparticles 19
3.4 Cell Culturing 19
3.5 Dark Toxicity Measurement 20
3.6 Comparison of the Dark Toxicities 21
3.7 Photodynamic Therapy (PDT) Experiments 22
3.8 Cellular Uptake Experiment 23
3.9 Investigating the Primary PDT Mechanism 25
3.10 ROS Production with DPBF Assay 26
3.11 Photodynamic Stability Experiment 27

3.12 Statistical Analysis 27
4. RESULTS 28
4.1 Characterization of Nanoparticles 28
4.2 Dark Toxicity Result 29
4.3 Determination of loaded amount of ZnPc into the ZnPc-MSN 30
4.4 Cellular Uptake 33
4.5 PDT Experiment Result 34
4.6 Primary Singlet Oxygen Generation Mechanism 35
4.7 ROS Production DPBF Experiment Result 37
4.8 Stability Experiment Result 38
5. DISCUSSIONS 40
6. CONCLUSION 43
REFERENCES 44

LIST OF FIGURES

Figure 2.1 The administration mechanism of PDT is illustrated schematically. PS is administered, and after adequate time for it to accumulate in the cancer, light is delivered to generate ROS, leading to cell death. 7

Figure 2.2 A schematic representation of the photochemical mechanism pathways of PDT, laser light irradiation, PS excitation, reactive oxygen species, and singlet oxygen production. PS_{ES}: PS at excited singlet state; PS_{ET}: PS at excited triplet state. 8

Figure 2.3 Illustration of EPR effect. While molecules remain in circulation in healthy vascular structures, they are taken into the tumor and retained in the tumor tissue due to the permeability of tumor vessels and low lymph drainage near the tumor. 11

Figure 2.4 Molecular Structure of ZnPc 12

Figure 2.5 A schematic representation of light penetration into the skin shows the depth to which wavelengths penetrate the skin. Red light can reach approximately 4-5 mm below the skin. 13

Figure 2.6 A schematic illustration of the mainly subcellular localization of ZnPc. 14

Figure 3.1 Illustration of MSN (a), ZnPc-MSN (b). 17

Figure 3.2 After the first (left) and second (right) washing steps of MSNs. 18

Figure 3.3 ZnPc loading process into the MSN on the magnetic stirrer, and after washing. 18

Figure 3.4 The A-549 lung cancer cells with 10x magnification. Scale bar: 200 μm. 20

Figure 3.5 Illustration of 96-well plate seeding scheme for dark toxicity experiment.Each group was seeded as six technical replicates. 20

Figure 3.6 Illustration of 96-well plate seeding scheme for comprehensive dark toxicity of ZnPc and ZnPc-MSN.Each group was seeded as six technical replicates. 21

Figure 3.7	Illustration of 96-well plate seeding scheme for PDT experiment, the black cover was always used for groups not currently illuminated. Each group was seeded as four technical replicates.	22
Figure 3.8	PDT experimental setup, with 600 nm LED light source.	23
Figure 3.9	Illustration of 6-well plate seeding scheme for cellular uptake experiment.	23
Figure 3.10	Falcon tubes before and after accumulated ZnPc extraction.	25
Figure 3.11	Illustration of 96-well plate seeding scheme for investigating the primary PDT mechanism experiment. Each group was seeded as four technical replicates.	25
Figure 4.1	DLS Result of MSNs.	28
Figure 4.2	MSNs STEM Images demonstrates the physical characterization, scale bars 500 nm, and 200 nm respectively.	29
Figure 4.3	Survival fraction result of A-549 cells incubated with different ZnPc-MSN concentration. Data for each group were normalized to the corresponding untreated controls (ns:no significant).	30
Figure 4.4	Standard curve of ZnPc measuring absorbance values of 20-500 μg/mL.	31
Figure 4.5	Absorbance spectrum of ZnPc (70.2 μg/mL) and ZnPc-MSN (2000 μg/mL).	32
Figure 4.6	Dark toxicity survival fraction of A549 cells treated with ZnPc (70.2 μg/mL) and ZnPc-MSN (2000 μg/mL). Data for each group were normalized to the corresponding untreated controls (ns:no significant).	33
Figure 4.7	Cellular uptake results of ZnPc and ZnPc-MSN.Significant difference marked by (***) (p =0.0007).	34
Figure 4.8	Survival Fraction of A549 incubated with ZnPc-MSN and light, only light and only ZnPc-MSN, light irradiation performed with 100 mW/cm^2 and at 660 nm. Data for each group were normalized to the corresponding untreated controls. Significant difference marked by (**) (p $<$ 0.05).	35

Figure 4.9 Dark toxicity survival fraction of 50 mM Sodium Azide in A-549 cells.Data for the group were normalized to untreated control(ns:no significant). 36

Figure 4.10 Survival fraction of A-549 cells after incubation with and without sodium azide, light irradiation performed with 100 mW/cm^2 and at 660 nm. Data for each group were normalized to the corresponding untreated controls.Significant difference marked by (**) ($p < 0.05$). 37

Figure 4.11 ZnPc 70.2 μg/mL and ZnPc-MSN 2000 μg/mL with 50 μ/M DPBF in DMSO absorbance change at 420 nm wavelength. 38

Figure 4.12 Photostability of ZnPc and ZnPc-MSN during 14 days, absorbance at 660 nm. 39

Figure 4.13 Photostability comparison of ZnPc and ZnPc-MSN for at 0 and 14 days, absorbance at 660nm. 39

LIST OF SYMBOLS

$^1O_2$	Singlet Oxygen
mW/cm^2	Milliwatts per Square Centimeter
J/cm^2	Joules per Centimeter Square
μg/mL	Microgram per Milliliter
O_2	Oxygen
CO_2	Carbon Dioxide
mM	Millimolar
mL	Milliliter
nm	Nanometer
M_{ZnPc}	Molar Weight of ZnPc
$\phi\Delta$	Singlet oxygen production capability
ϕ	Triplet quantum yields
τT	Triplet Lifetimes
ET	Excited Triplet
ES	Excited Singlet

LIST OF ABBREVIATIONS

ANOVA	Analysis of Variance
CTAB	Cetyltrimethyl Ammonium Bromide
DI Water	Deionized Water
DLS	Dynamic Light Scattering
DMEM	Dulbecco's Modified Eagle Medium
DMF	Dimethylformamide
DMSO	Dimethyl Sulfoxide
DOX	Doxorubicin
DPBF	1,3-Diphenylisobenzofuran
ER	Endoplasmic Reticulum
EPR	Enhanced Permeability and Retention
FBS	Fetal Bovine Serum
FDA	US Food and Drug Administration
GA	Golgi Apparatus
HpD	Hematoporphyrin Derivatives
LED	Light Emitting Diode
MOS	Mesoporous Organosilica Nanoparticle
MPR	Microplate Reader
MSN	Mesoporous Silica Nanoparticle
MTT	3-(4,5-Dimethylthiazol-2-yl)-2,5-Diphenyltetrazolium Bromide
NIR	Near Infrared Radiation
NSCLC	Non-Small Cell Lung Cancer
PBS	Phosphate Buffered Saline
Pcs	Phthalocyanine
PDT	Photodynamic Therapy
PEG	Polyethylene glycol
PEI	Polyethyleneimine
PS	Photosensitizer

PTT	Photothermal Therapy
ROS	Reactive Oxygen Species
SCLC	Small Cell Lung Cancer
SMSNs	Stella Mesoporous Silica Nanoparticles
STEM	Scanning Transmission Electron Microscope
TEOS	Tetraethyl Orthosilicate
TGP	Triangular Gold Nanoprism
UV-Vis	UV-Visible Spectroscopy
UCNP	Upconvertion Nanoparticles
WHO	World Health Organization
ZnPc	Zinc Phthalocyanine
ZnPc-MSN	Zinc Phthalocyanine incorporated Mesoporous Silica Nanoparticle

1. INTRODUCTION

Cancer is regarded as the second reason of death worldwide; according to the American Cancer Society, 611,720 expected deaths in the United States are caused by cancer [1]. Conventional cancer treatment methods include chemotherapy, surgery, and radiotherapy; however, such therapies may not be effective and cause severe side effects [2].

PDT is considered one promising cancer therapy option that uses two essential components: PS and an appropriate light source (usually laser). In this method, PS is administrated, and after the accumulation of PS in the tumor, which can happen either by passive targeting or by using active targeting approaches, the tumor is illuminated with a laser beam. This interaction yields cytotoxic ROS in the tumor [3],[4].

An ideal PS should be nontoxic without laser irradiation and demonstrate high absorbance in the therapeutic window, which is determined to be nearly 600-850 nm due to deeper light penetration in this wavelength range. The PS molecules should be quickly cleared from healthy tissue. Furthermore, since the essential part of PDT is producing ROS, PSs should generate a high level of ROS after laser irradiation. Additionally, selectivity is a substantial criterion for PS; therefore, the PS molecules should accumulate in the tumor [4],[5].

ZnPc is a second-generation PS. ZnPc is stable compared to other PSs and demonstrate high absorbance (660-680 nm) at the UV-Visable region. It generally accumulates in mitochondria, which can induce cell death via apoptosis when it is damaged. On the other hand, ZnPc has low water solubility, which limits its usage in PDT [6]. To overcome this limitation, drug delivery systems can be used. Although ZnPc-loaded nanoparticle drug delivery is a promising option for use in PDT of cancer, the literature lacks adequate investigations into the effectiveness of ZnPc-based nanoparticles in different in vitro models. In this study, MSNs, which are biocompati-

ble and easy to functionalize, are preferred, and the effectiveness of MSN incorporated ZnPc was evaluated on lung cancer cells [7].

1.1 Motivation and Objectives

PDT is considered one promising cancer therapy, which utilizes photochemical agents that generate ROS that target cancer cells upon exposure to appropriate light wavelengths [4].

ZnPc, a second-generation PS, is constrained by its low solubility, cellular uptake, and tumor selectivity [8]. With its large surface area, adjustable pore size, and compatibility with biological systems, MSNs can potentially enhance the effectiveness of PDT by addressing issues with aqueous solubility and targeted cargo delivery [7].

The study aims to research the efficacy of PDT with ZnPc-MSN systems on the A549 lung cell line. Also, we investigated the synthesized MSN's characteristics and measured the amount of ZnPc loaded into the nanoparticles. The primary PDT mechanism and stability of ZnPc-MSN were also examined. In vitro experiments were conducted on the A549 cells to investigate cellular toxicity, uptake, and PDT effects.

2. BACKGROUND

2.1 Lung Cancer

Cancer is a dramatically fatal disease that affects people across the world. According to the American Cancer Society, it is predicted that by the year 2024, there will be approximately 2,001,140 additional cancer cases and 611,720 cancer-related deaths in the United States. Lung cancer is projected to be the second most common cancer type for both women and men, with 118,720 cases among women and 116.310 among men. The estimated percentage of lung cancer-related deaths is 21% for women (59,280) and 20% for men (65,790) [1].

Lung cancer develops in the lung parenchyma or within the bronchial tubes. Its pathophysiology is highly complicated. Exposure to carcinogens such as cigarette smoke thought to caused lung epithelial dysplasia, which interferes with the normal cell division progression and provokes cancer formation [9].

Primary lung cancer refers to cancer that originates within the lung itself. In contrast, secondary lung cancer refers to cancer that has metastasized to the lungs from another part of the body [10],[11]. While primary lung cancer encompasses several types, according to WHO, they are primarily classified into two main categories: non-small cell lung cancer (NCSLC) and small cell lung cancer (SCLC) [10],[12].

In the United States, over 30,000 new SCLC cases are determined annually, and SCLC constitutes 14% of all lung cancers [10]. SCLC frequently exists as a perihilar mass, and it is found in a peribronchial position characterized by infiltration into the bronchial submucosa and surrounding peribronchial tissue. [10],[13]. According to the World Health Organization (WHO), the categorization of SCLC has two variations: SCLC (consisting of pure SCLC) and combined SCLC (including any NCSLC). SCLC exhibits unique characteristics, including a threatening clinical progression, ex-

tensive metastases often seen at diagnosis, and frequent occurrence of paraneoplastic syndromes [10]. For patients in advanced stages, despite the application of combined therapy involving chemotherapy and radiotherapy, the average survival is 15 months, with only a 10% at the 5-year mark [10],[14].

NCSLC represents 80-85% of all diagnosed lung cancer cases. The three primary subtypes include squamous cell carcinoma, large cell carcinoma, and adenocarcinoma [11]. Adenocarcinoma in the United States, adenocarcinomas account for 38% of all lung cancer cases [10]. Lung adenocarcinoma typically arises from the mucosal glands and frequently emerges in the peripheral regions of the lung [15].

Lung squamous cell carcinoma (SCC) frequently arises in the middle portion of the lung or within a central airway, like the right or left bronchus. Compared to other types of NSCLC, smoking has a stronger correlation with SCC [16].

2.2 Treatment of Lung Cancer

Adenocarcinoma, squamous cell carcinoma, and large cell carcinoma are subtypes of NSCLC, which makes up 85% of all instances of lung cancer. The therapeutic objectives for NSCLC patients vary based on the disease stage. Those in stages I through III seek a cure, whereas for patients in stages IV, goals involve alleviating symptoms and extending life expectancy. To decide on appropriate treatment options, it is essential to determine the tumor's location and whether and where metastases are present [17].

According to the stage of cancer, several treatment options can be addressed, such as surgery, gene therapy, chemotherapy, or radiotherapy. The primary treatment for early-stage NSCLC is surgical resection, supplemented by adjuvant chemotherapy given to specific individuals. Combination therapy, typically involving synchronized chemotherapy and radiation, is used to treat stage III NSCLC to cure it. Chemotherapy and radiation therapy are the predominant approaches focusing on symptom alleviation

of advanced NSCLC, which is still incurable. Additionally, patients with progressed NSCLC with special genetic alterations can significantly utilize molecularly targeted therapy [17].

SCLC represents a formidable malignancy marked by its neuroendocrine development, propensity for early metastasis, and initial therapeutic responsiveness [13]. Additionally, brain metastases are prevalent in SCLC, with approximately 10% of those having brain metastases at the initial diagnosis [16]. Constituting approximately 15% of all lung cancer diagnoses, SCLC presents a significant challenge in clinical management and underscores the urgency for effective treatment strategies [17],[18]. SCLC is commonly staged utilizing the Veterans' Administration Lung Group categorization system, which is the limited stage (LS) and extensive stage (ES) disease [13].The LS disease is referred to by the tumor that is limited to one hemithorax and may be safely covered by a single radiation port. This indicates that the cancer is restricted to one lung or may involve nearby lymph nodes [17],[19].

Although most patients diagnosed with locally progressed disease are locally progressed, a few percent may have early stages. A lobectomy combined with dissection or mediastinal sampling may be appropriate for these patients. In cases where surgery reveals involvement of mediastinal lymph nodes, adjuvant chemotherapy concurrent radiotherapy is recommended. Stereotactic ablative radiotherapy (SABR) may be utilized for those not eligible for surgery. Additionally, both local strategies can be employed in neoadjuvant-based cisplatin systemic therapy [20],[21].

Radiation and chemotherapy are administered concurrently to the rest of limited-stage patients. The standard of care at the moment is etoposide and cisplatin. Radiation therapy significantly improves overall survival and local control when combined with chemotherapy. It has been demonstrated that, in comparison to late inclusion, early radiotherapy with chemotherapy increases overall survival. Patients who respond entirely or partially to therapy should receive prophylactic cranial irradiation (PCI). It dramatically diminishes the incidence of brain metastases and improves overall survival [21],[22].

Systemic chemotherapy is the cornerstone of treatment for those in extensive stages [19]. Radiotherapy is typically used to alleviate symptoms in patients who have progressed to a stage where they are unable to respond sufficiently to chemotherapy. In addition, there has been a correlation between the therapy's increased overall survival and is well-tolerated. PCI has been correlated with attenuation in the percentage of brain metastases and improved patients' survival rates [20],[21].

Multiple studies have shown that the addition of an immune checkpoint inhibitor to first-line chemotherapy offers statistically significant advantages for patients with recently identified metastatic SCLC [23],[24]. Targeted cancer treatments and immunotherapies are promising options for both NSCLC and SCLC [20].

Conventional cancer treatments include chemotherapy, surgery, or radiotherapy; however, such therapies may not eradicate tumors and cause serious side effects [2]. Traditional treatments may pose lack of selectivity, multidrug resistance, and complications caused by surgery [20]. To deal with these problems, researchers have focused on finding new advanced, effective, and minimally side-effective cancer treatments. Photoactive therapies like PDT are attractive since they use nonionizing radiation and can achieve selective targeting therapy [4].

2.3 Photodynamic Therapy

PDT can be defined as a light-activated treatment modality, and it is also a minimally invasive or non-invasive treatment for cancer and other illnesses [25]. It requires a nontoxic phototherapeutic agent, which can be activated by laser irradiation with appropriate wavelength (generally UV-Vis and near-infrared region (NIR)) to trigger cancer cell death [26]. The PS can accumulate in cancer cells. An appropriate wavelength laser is applied to the desired area, and this interaction with PS generates ROS that are toxic to tumor cells. The cancer treatment mechanism of PDT can be classified into three main concepts: the production of ROS, the extermination of tumor blood vessels, and the triggering of the immune system against cancer cells [27].

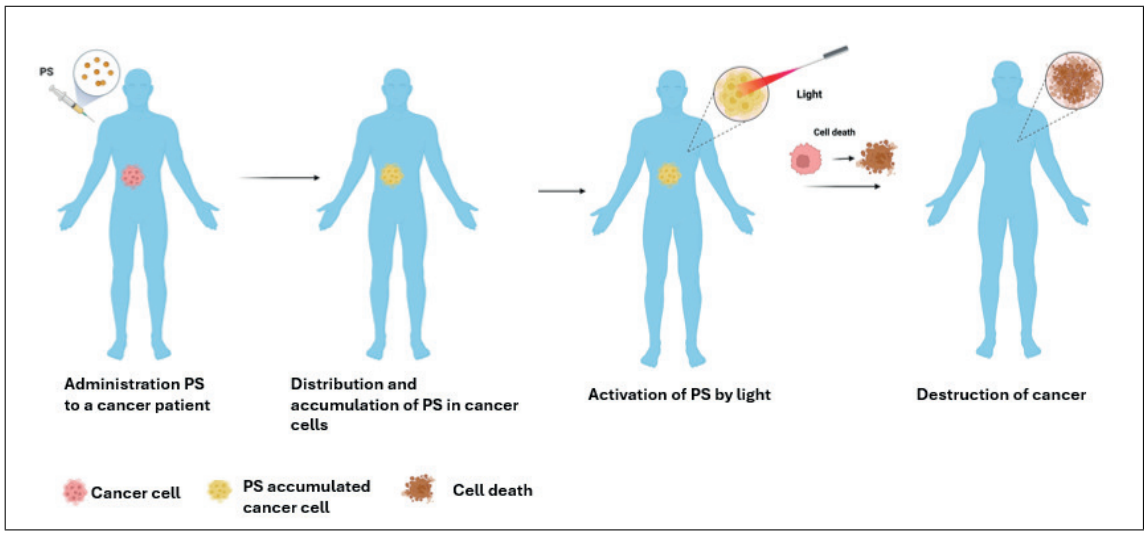


Figure 2.1 The administration mechanism of PDT is illustrated schematically. PS is administered, and after adequate time for it to accumulate in the cancer, light is delivered to generate ROS, leading to cell death.

The molecular mechanism of PDT depends on three components: PS, light with a specific wavelength, and ROS, and the interaction between these components allows toxic effects on the target tissue [28]. The photodynamic reaction has two fundamental mechanisms closely related to the oxygen molecules inside the cells. After being accumulated by the tumor, the tissue is exposed by a laser with a specific wavelength. When the PS absorbs light, the molecules are excited from the ground to the singlet excited state. PS can return to the ground state by emitting fluorescence, or the PS molecule can make an intersystem crossing to the triplet excited state, which leads to relaxation that causes the creation of ROS [4]. The relaxation of the PS from the excited triplet state to the ground state can lead to two types of reactions, Type I and Type II [29].

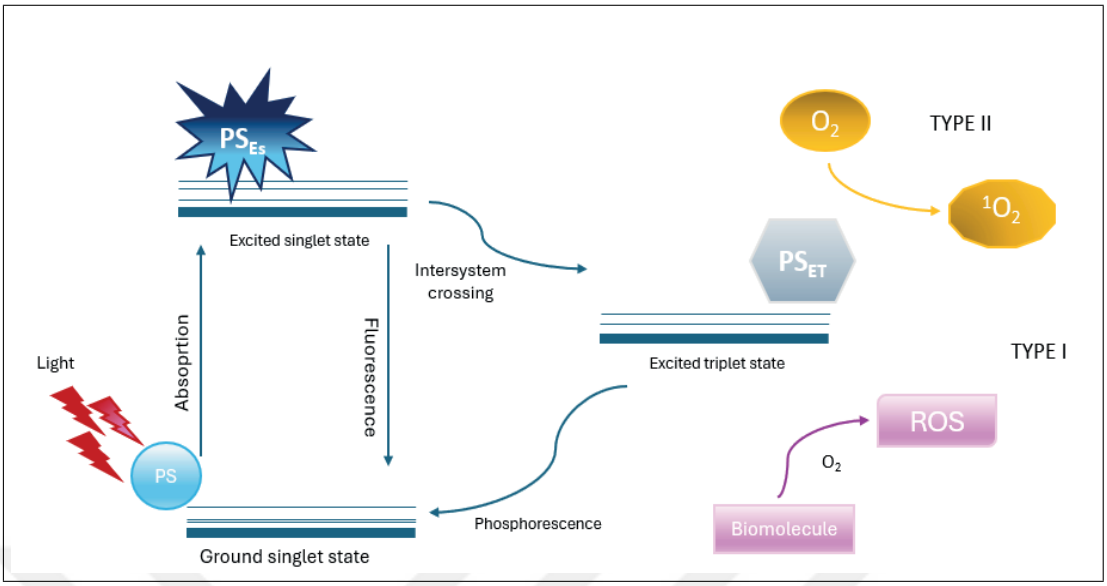


Figure 2.2 A schematic representation of the photochemical mechanism pathways of PDT, laser light irradiation, PS excitation, reactive oxygen species, and singlet oxygen production. PS_{ES}: PS at excited singlet state; PS_{ET}: PS at excited triplet state.

In Type I reactions, the PS can donate or receive electrons to the biomolecules, generating free radicals, which leads to the generation of ROS after other chemical reactions [30].

In the Type II mechanism, PS can directly transfer energy to the oxygen molecule since they have the same spins. As a result, singlet oxygen is produced, demonstrating powerful oxidizing features [4],[30]. Furthermore, since singlet oxygen only lasts about three milliseconds in cells, any damage is concentrated in a small area, causing permanent damage to cancer cells while sparing surrounding healthy cells [31]. The increased ROS in the target tissue produces the photodamage of proteins, fat, and other structures in the desired area. These interactions can eradicate cancer cells in necrosis and apoptosis [32]. Additionally, subcellular localization of PS can cause mitochondria damage, leading to apoptosis, cell membrane destruction, and loss of unity, which can trigger necrosis. Autophagy can also be induced by damaging the endoplasmic reticulum or lysosomes [33].

2.4 Photosensitizers

The characteristics of PS affect the effectiveness and safety administration of PDT. It should be nontoxic without light irradiation, and demonstrate high absorbance in the therapeutic window, which is determined nearly 600-850nm to allow deeper penetration ability. Additionally, PSs should have high ROS generation capacity to trigger cytotoxicity in the cancer tissue after irradiation of light [4],[34]. The selective targeting ability ensures optimal accumulation in the cancerous tissue as well as limitations in the healthy ones and provides rapid elimination from the body, diminishing possible undesirable long-term effects. Another property is solubility, which enables the distribution of the body for convenient administration. The combination of these properties increases the overall efficacy of PDT [27],[35].

Porphyrins and hematoporphyrin derivatives (HpD) are examples of the first PSs used in PDT. Although they destroy cancer cells by ROS production, some features restrict their usage, such as lacking adequate light absorption and targeting ability, as well as exhibiting skin sensitivity [34].

To overcome those limitations, second-generation PSs, phthalocyanines, porphyrins, and chlorins were recognized [4]. In 1907, Braun and Tcherniac synthesized phthalocyanines (Pcs) [8]. The Pcs become promising for PDT thanks to their characteristics, including high absorbance in the therapeutic window at 600-800 nm, allowing deep tissue penetration, and having high singlet oxygen quantum yields which indicate effectively triggering cellular destructions exposed to light [36],[37].

Pcs are aromatic macrocyclic molecules in which four isoindoline agents are bonded with nitrogen atoms. In the UV-Vis spectrum, they exhibit absorbance approximately 350 nm in the Soret band while near 680 nm in the Q band. The molar extinction coefficient of $1x10^5 M^{-1} cm^{-1}$ distinguishes these from most porphyrins. The photochemical properties of Pcs are significantly affected by the coordinated central ion, and these properties can be enhanced by modification of their chemical structure. The presence of diamagnetic metals like gallium, zinc, and aluminum as the center ion

can significantly affect singlet oxygen production capability ($\phi\Delta > 0.4$) by providing high triplet quantum yields (ϕ T$>$ 0.4), increased triplet lifetimes (τ T$>$ 100 μs) and excited triplet energies (ET = 1.2 eV) [8],[38],[39].

The nanoparticle drug delivery system in PDT has attracted attention as it enables the delivery of hydrophobic drugs and has demonstrated sufficient accumulation into the cancer cells. For instance, liposome nanoparticles successfully capture hydrophobic drugs, preventing their degradation and improving their solubility in the cellular environment [8]. Besides, silica nanoparticles are a promising approach for delivering PS to cancer cells as they provide a durable structure for the cargo and demonstrate their versatility, enabling selective drug delivery through significant surface modification alternative [6]. Third-generation PSs are being investigated to improve the safety and efficacy of PDT in clinical applications. To interact with cancer cells, they are constructed using additional moieties to second-generation PSs, such as antibodies and peptides. Moreover, the advanced design may enable synchronized diagnosis and therapy to serve real-time treatment [40],[41].

Research is ongoing to develop ideal PSs to increase the efficacy and safety of PDT in cancer treatment.

2.5 Nanoparticles in Photodynamic Therapy

Nanoparticles can be preferred as an adjuvant in drugs or vaccine carriers where the drugs or phototherapeutic agents are encapsulated, chemically linked, absorbed, engaged, or solved [42],[43]. Each type of nanoparticles has distinguished morphology, construction, and dimension. These variations offer unique benefits depending on the application area [44]. Furthermore, nanoparticles protects the drug from enzymatic degredation and other environmental conditions [45].

An essential component of PDT effectiveness is the efficient localization of PS at the target site. Loading drugs into nanoparticles enhances the localization to the

target area. Although no specific active targeting is used, nanoparticles can accumulate at target sites through passive targeting, the EPR effect [46].

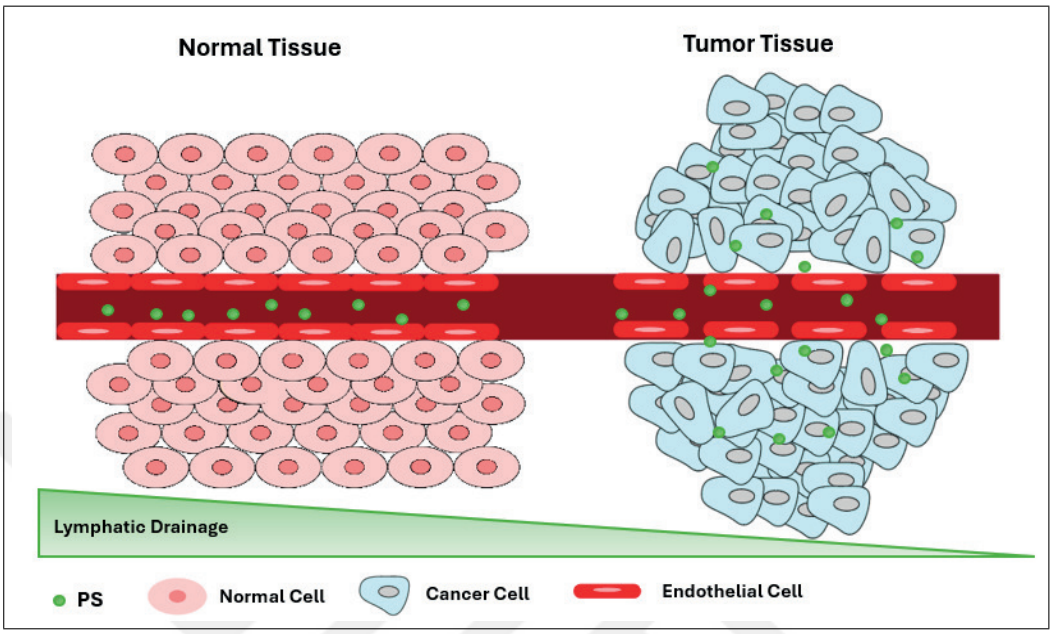


Figure 2.3 Illustration of EPR effect. While molecules remain in circulation in healthy vascular structures, they are taken into the tumor and retained in the tumor tissue due to the permeability of tumor vessels and low lymph drainage near the tumor.

The EPR effect, a crucial factor in tumor-targeting drug delivery systems, exploits the anatomical differences between tumor tissue and normal tissue. This effect is significant in cancer treatment as it allows for the selective delivery of drugs to tumor sites [47].

Compared to the vascular network in normal tissue, tumor blood vessels have imperfect large pores, resulting in less selective permeability and less selectivity to supply the nutrients and oxygen needed to sustain rapid growth [47],[48]. The EPR effect utilizes this inherently defective vascular system of the tumor to ensure the delivery of macromolecules to the tumor side. Sizing more than 40 kDa, the threshold for renal clearance causes specific leakage from tumor arteries and increases the localizing of macromolecules in the tumor. In contrast, another advantage of the passive targeting system, a drug delivery approach that relies on the EPR effect and does not require active intervention, is that drug accumulation is less in normal tissue [47].

Additionally, these macromolecules increased plasma half-life, providing target selectivity. This phenomenon has led to significant advances in creating enhanced PS delivery systems to improve target localization for effective cancer therapy [47],[48].

2.6 Zinc Phthalocyanine

Zinc phthalocyanine (ZnPc) is one of the metallophthalocyanine species, a second-generation PS in which zinc is bonded to four isoindole groups as the central ion conjugate, resulting in a planar conjugated ring chemical structure [8],[49].

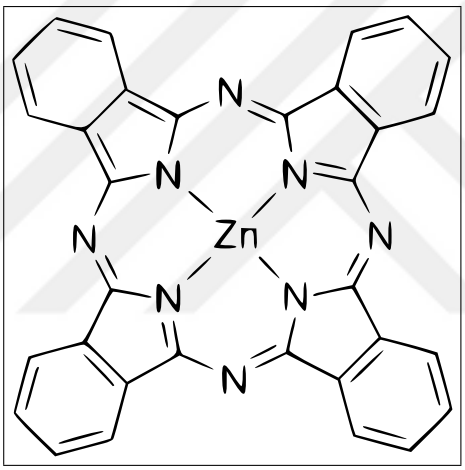


Figure 2.4 Molecular Structure of ZnPc [8].

The ZnPc exhibits valuable properties including potent photostability, low cytotoxicity without light irradiation, and having strong absorption at 660-680 nm which provides desired tissue penetration depth,in the range of 4-5 mm [8],[50].

Furthermore, ZnPc has a high $\phi\Delta$ 0.67 in dimethyl sulfoxide (DMSO) [51]. This forms a long-lasting triplet state and has significant cytotoxic effects by inducing cell death upon exposure to light, thus resulting in an effective PDT [52],[53].

According to literature, mitochondria and lysosomes are the primary sites for the subcellular accumulation of ZnPc. Depending on the incubation time and cell line

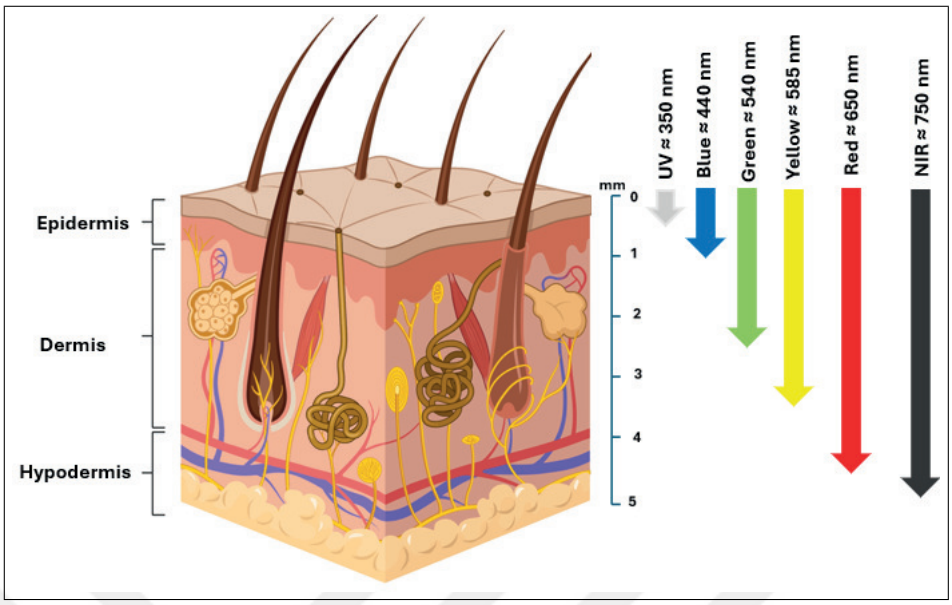


Figure 2.5 A schematic representation of light penetration into the skin shows the depth to which wavelengths penetrate the skin. Red light can reach approximately 4-5 mm below the skin.

type, it can also localize in the endoplasmic reticulum (ER), Golgi apparatus (GA), or plasma membrane [8],[54].

Velazquez et al. evaluated PDT efficacy of ZnPc and Zn(II)tetraminephthalocyanine (TAZnPc), which is derivative of ZnPc, on three different glioblastoma cell lines. In this study, the authors examined the dark toxicity, cellular uptake and subcellular localization of the PS. In conclusion they indicate that both PS with light exposure can induce successfully cell death by apoptosis [54].

Soriano et al. investigated the cellular uptake performance of ZnPc into A-549 adenocarcinoma cells with two distinguishing administration methods, ZnPc-DMF, which dissolve in dimethylformamide (DMF) and ZnPc-liposomes. The study analyzed the dark toxicity at different incubation times, subcellular localization, cellular uptake, and PDT effects. They demonstrated that these PSs are mainly found in mitochondria. As a result, the authors indicated that ZnPc-DMF is adjoined into A-549 cells through caveolin-guided endocytosis, whereas ZnPc-lipo is uptake by cell utilizing endocytic method based on clathrin, and both PS demonstrated meaningful cell death triggered when exposed to light [55].

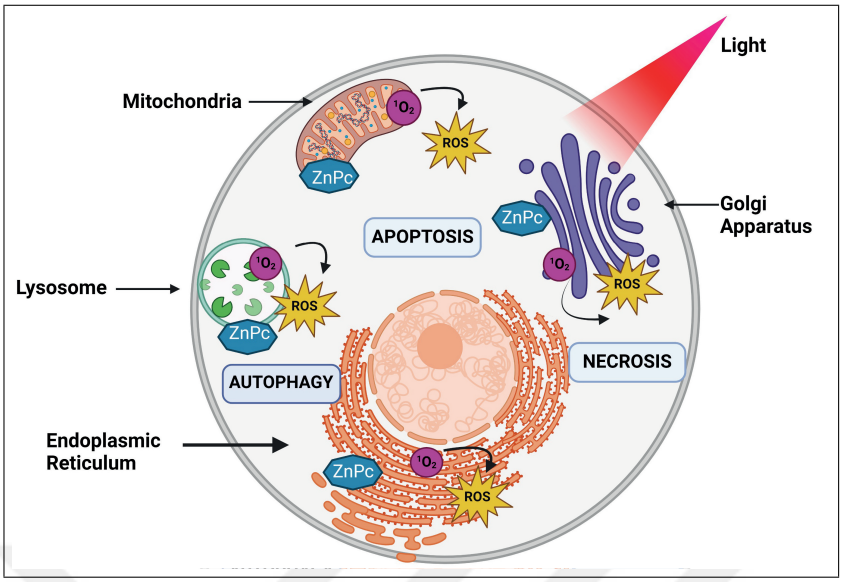


Figure 2.6 A schematic illustration of the mainly subcellular localization of ZnPc.

Chen et al. synthesized novel Pcs called Photocyanine (Shutalazin), derivatives from ZnPc. The new compound consists of four sulfonate isomers of di-(potassium sulfonate)-di-phthalimidomethyl Pcs zinc (ZnPcS2P2), which the chemical structure allowing amphiphilicity, thereby can easily administration bloodstream and elevated accumulation in the cancer cells. The absorbance of Photocyanine is 675 nm in DMF. Additionally, singlet oxygen and fluorescence quantum yield are defined as 0.53 and 0.26, respectively, which means that light exposure can induce cell death. The results of the comprehensive experiment indicate that Photocyanine shows remarkable therapeutic effects even though the dose is ten times lower than that of Photofrin, which is an HpD derivative PS in clinics. Low dose administration can reduce the risk of treatment. In addition, preclinical study results of Photocyanin have led to its approval for clinical trials by the China Food and Drug Administration, and phase II clinical trials will be conducted for esophageal cancer [56],[57].

2.7 Mesoporous Silica Nanoparticles

The US Food and Drug Administration (FDA) acknowledges silica as safe and preferred in ingredient medications [58]. MSNs are considered important drug trans-

porters thanks to features that include easy synthesis, biocompatibility, adequate surface area, and tunable pores, allowing effective loading of various cargo types (PSs, drugs, dyes) without destabilization of silica skeleton, which protects the cargo from enzymatic degradation and prevents its inactivation by plasma molecules [7].

Intravenous administration of hydrophobic cargos is restricted due to their low water solubility, and they require high amounts of organic solvents such as DMSO, which are toxic to cells. On the other hand, silanol groups on the MSN make them hydrophilic, and their large surface and pore volumes can accommodate drug molecules to transport hydrophobic cargo in the bloodstream. Besides covalent interactions, drugs can adhere to MSN by way of physical adsorption, including electrostatic forces and hydrogen bonding. These interactions lead to both the efficiency of loading and providing successful release. Additionally, drugs can maintain stability and do not dissolve in aqueous biological media after loading. In vitro investigations suggest that particle interactions with cell membranes and phospholipids can allow the release of encapsulated hydrophobic drugs during endocytosis. Surface modification of MSNs can increase drug accumulation in therapeutic targets, preventing premature release in the bloodstream [5],[7],[59].

Tu et al. constructed a ZnPc-loaded MSN delivery system modified with PEG and PEI to improve biocompatibility and endosomal escape efficiency. The study indicates that PEG-PEI-MSNs/ZnPc exhibit a significantly higher escape efficiency from the ZnPc- MSNs. Additionally, in vivo PDT experiment results exhibit successful cell death with laser exposure and adequate PS accumulation on the cancer cells thanks to the EPR effect [6].

Lin et al. created a pH-responsive PS consisting of ZnPc-loaded stellate mesoporous silica nanoparticles (SMSNs). The singlet oxygen generation capacity of inactivated ZnPc-SMSNs is quenched, and it can regain generation capacity inside the acidic medium, like a tumor microenvironment. In vitro experiments on HeLa cells showed successful ROS production and phototoxicity when exposed to light. Furthermore, in vivo experiments have shown that intravenous administration of the compound resulted

in selective targeting of the tumor and inhibits tumor growth [60].

Liu et al. synthesized TGP-MOS, a triangular gold nano prism core coated with encapsulated ZnPc mesoporous organosilica (MOS). They evaluated combined photothermal therapy (PTT) and PDT in in-vivo and in-vitro experiments. This study demonstrated successful ZnPc encapsulation thanks to aromatic interactions with the MOS shell. Combination therapy triggered single laser irradiation, which is mediated by heat increasing from the TGP core, leading to PTT and PDT, driven by ROS generation from ZnPc, which synergistic therapies induced cell death. This study suggests the condition of TGP-MOS-ZnPc as a core-shell nanoplatforms for an effective method of breast cancer treatment [61].

Ma et al. developed doxorubicin (DOX) and ZnPc co-encapsulate MSNs covered with a middle layer of calcium phosphate (CaP), and the outer layer is composed of PEGylated liposomes. CaP provides a controlled release of drugs by degrading in the acidic environment of tumors and can initiate apoptosis in cancer cells by facilitating the elimination of nanoparticles. Liposomes increase biocompatibility and drug delivery, while PEGylation prolongs circulation time in the bloodstream. ZnPc damages cancer cells via PDT upon light irradiation. This design combines the established efficacy of chemotherapy with the targeted action of PDT, offering a promising strategy for collaborative cancer therapy [62].

Furthermore, MSNs can encapsulate other nanoparticles for drug loading. Qian et al. developed a PS in which ZnPc was physically absorbed into the pores of MSN and coated upconversion nanoparticles (UCNPs). In this study synthesized nanoparticles demonstrated high stability and a successful PDT effect under laser irradiation. This UCNP-MSN-ZnPc presents a promising design for PDT nanoparticles, highlighting the increased tissue penetration depth and controlled drug delivery [63].

In conclusion, ZnPc-MSN drug delivery systems demonstrate advantages, including increased water solubility and enhanced cellular accumulation, leading to elevated overall PDT results [64].

3. MATERIALS AND METHODS

3.1 Synthesis of Mesoporous Silica

MSNs were prepared as previously detailed [65]. In summary, 7.5 mL of deionized (DI) water was combined with 1.057 mL of Ammonium-hydroxide (NH_4OH) on magnetic stirrer. The volume of the solution was then adjusted to 30 mL with an additional 21.44 mL DI water on magnetic stirring at 500 rpm and 40 ℃. Following this, 0.058 g of cetyltrimethylammonium-bromide (CTAB) was introduced and allowed to dissolve completely. 482 μL of ethanol and 118 μL of tetraethyl-orthosilicate (TEOS) were added consequently, the temperature was increased to 60 ℃, and the mixture was stirred at 500 rpm for two hours to precipitate the nanoparticles, the temperature change was regularly followed. After two hours, the nanoparticle mixture was centrifuged and sonicated, washing with ethanol three times. The precipitated nanoparticles were dissolved in 20 mL of ethanol, and 20 μL of hydrochloric acid (HCL) was added. It was stirred at 500 rpm and 60 ℃ for three hours. Finally, the MSNs were centrifuged and sonicated, washing with ethanol three times.

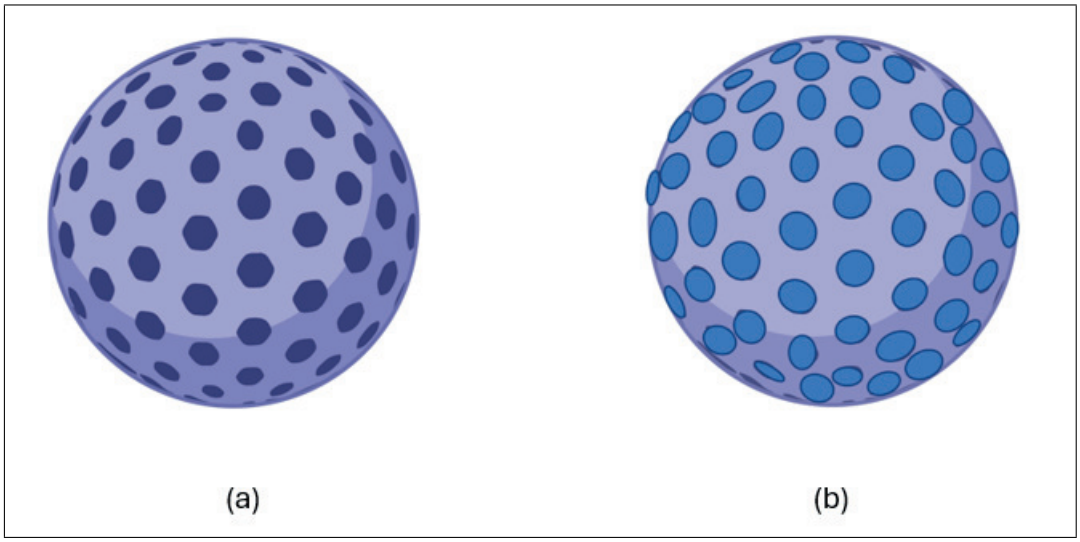


Figure 3.1 Illustration of MSN (a), ZnPc-MSN (b).

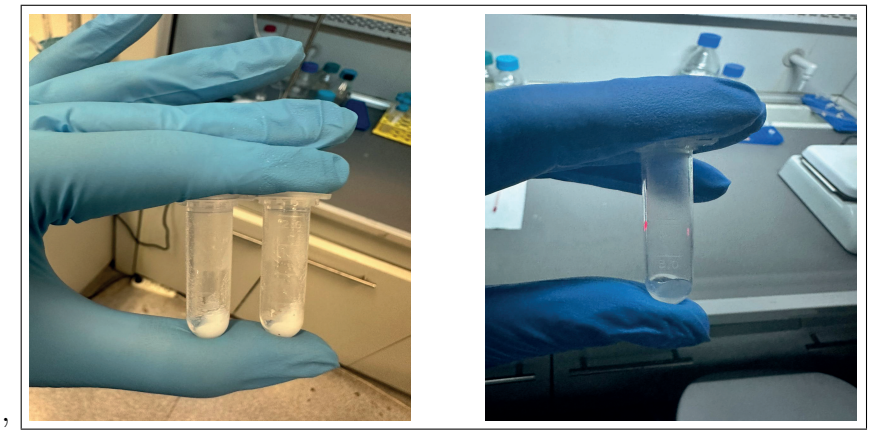


Figure 3.2 After the first (left) and second (right) washing steps of MSNs.

3.2 Loading ZnPc into the MSN

2 mg/mL ZnPc was completely dissolved in 20 mL DMSO and ethanol mixture using vortexing and magnetic stirring. Then, the synthesized MSN was added at 500 rpm and stirred at room temperature for 24 h. The following synthesized nanoparticles were centrifuged and washed with DI water two times. At the end of the synthesis, a 10 mg/mL concentration of ZnPc-MSN was obtained and kept at -20 ℃.

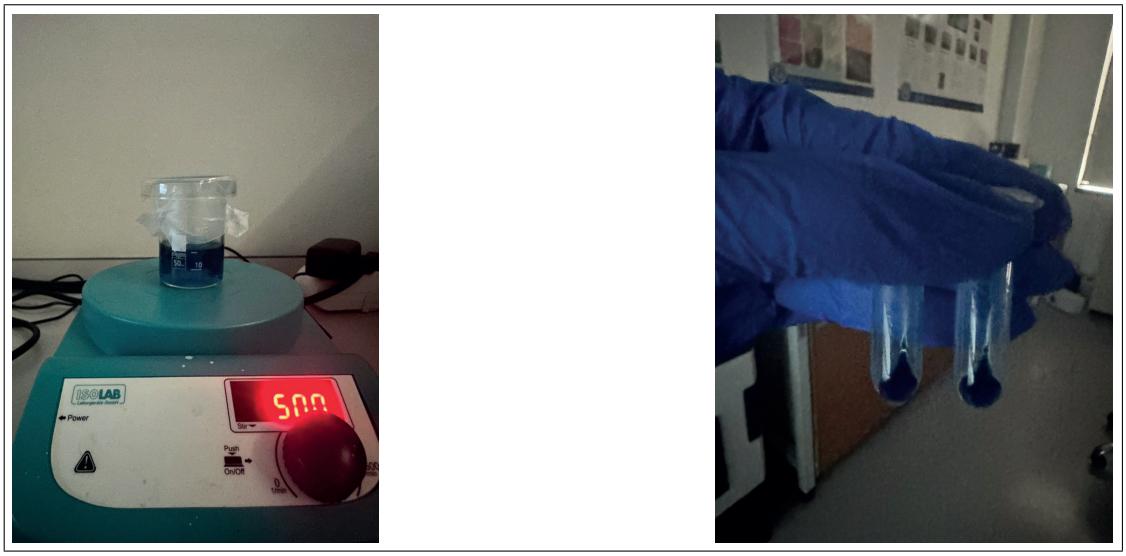


Figure 3.3 ZnPc loading process into the MSN on the magnetic stirrer, and after washing.

3.3 Characterization of Nanoparticles

Synthesized nanoparticles were kept in the incubator for 24 hours to determine the synthesized amount, approximately 15 mg weighed and dissolved in 1.5 mL ethanol, using a sonicator. A scanning transmission electron microscope (STEM) was utilized to visualize the shape and morphology of nanoparticles. Dynamic Light Scattering (DLS) was used to measure their size and intensity distribution. It is an effective method to figure out the size and spread of nanoparticles in a liquid. The working principle of DLS is based on measuring how much light intensity is reflected from the nanoparticles as a result of the random shaking of the nanoparticles (Brownian motion) by the impacts from the surrounding liquid molecules; DLS can measure the size of the nanoparticles based on this shaking [66]. The standard curve of ZnPc was calculated using the absorbance values of concentrations between 20-500 μg/mL at 655 nm wavelength utilizing a microplate reader(MPR) (BIO-RAD /iMark). The loading amount of ZnPc into the ZnPc-MSN was calculated using a standard curve equation.

3.4 Cell Culturing

In this study, the A549 human lung adenocarcinoma cell line was cultured, preserved at -80 ℃, and thawed in a 37 ℃ water bath. The Dulbecco's Modified Eagle Medium (DMEM) was supplemented with 10% fetal bovine serum (FBS) and 1% Penicillin-Streptomycin to obtain complete media. The thawed cell suspension was diluted with the complete medium and centrifuged. To clear away the DMSO, the supernatant carefully aspirated. The diluted cell solution was then transferred to T-25 flasks and incubated at 37 ℃ in 5% CO_2. Cell confluence was monitored, and the medium was replaced regularly. Upon reaching approximately 80%-90% confluence, subculturing was conducted by aspirating the old medium, washing the cells with sterile PBS, and adding trypsin-EDTA solution to facilitate cell detachment.

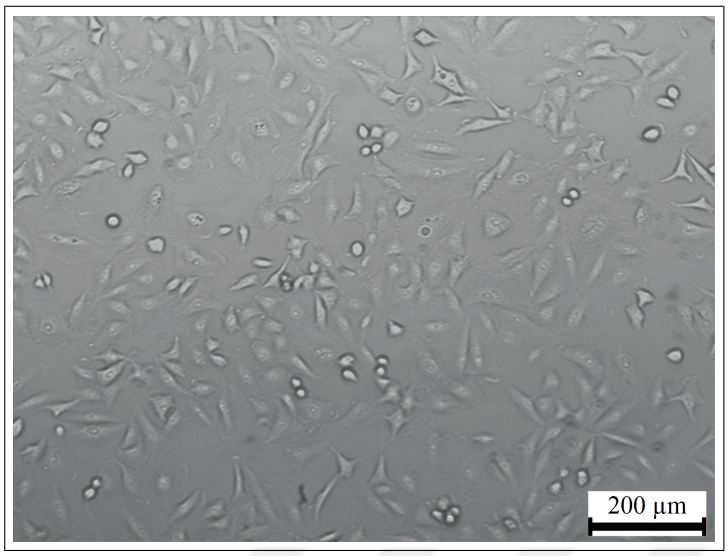


Figure 3.4 The A-549 lung cancer cells with 10x magnification. Scale bar: 200 μm.

3.5 Dark Toxicity Measurement

MTT (3-(4,5-dimethylthiazol-2-yl)-2,5-diphenyltetrazolium bromide) was used to assess the cytotoxicity of drug-loaded mesoporous silica nanoparticles. In the dark toxicity experiment, 1x10^4 cells were seeded into 96-well plates, with control and nine groups representing different concentrations of ZnPc-MSN, each applied as six technical replicates. After a 24-hour incubation, the cells were treated with 25, 50, 100, 150, 250, 500, 750, 1000, and 2000 μg/mL of ZnPc-MSN for 2 hours.

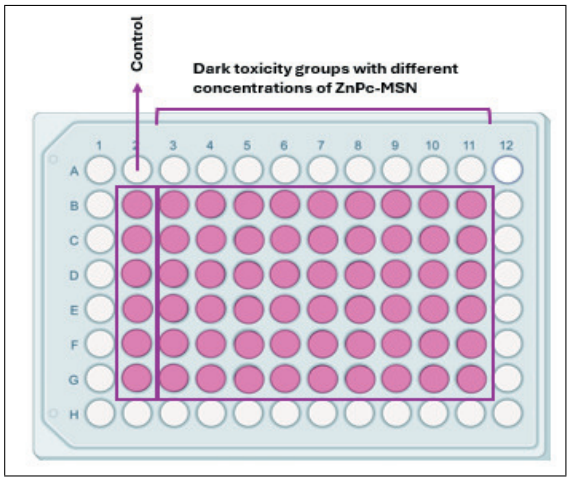


Figure 3.5 Illustration of 96-well plate seeding scheme for dark toxicity experiment.Each group was seeded as six technical replicates.

Following the 2-hour incubation, each well was washed with PBS for three times, and a fresh medium was added. After an additional 24 hours, MTT was applied to each well. The MTT was removed three hours later, and 100 μl of DMSO was added to each well. The results were then measured using the MPR. Three independent repeats were performed.

3.6 Comparison of the Dark Toxicities

To investigate the effect of the combination of ZnPc-MSN on the phototoxicity of free ZnPc, the phototoxicity of selected ZnPc-MSN concentrations alone will be compared with the phototoxicity of the same concentrations of free ZnPc used. Based on the measured absorbances, the amount of ZnPc loaded into MSN was calculated using the standard curve. ZnPc was dissolved in DMSO, which is known to be toxic to living cells at high concentrations, so DMSO was added as the experimental group for cytotoxicity analysis.

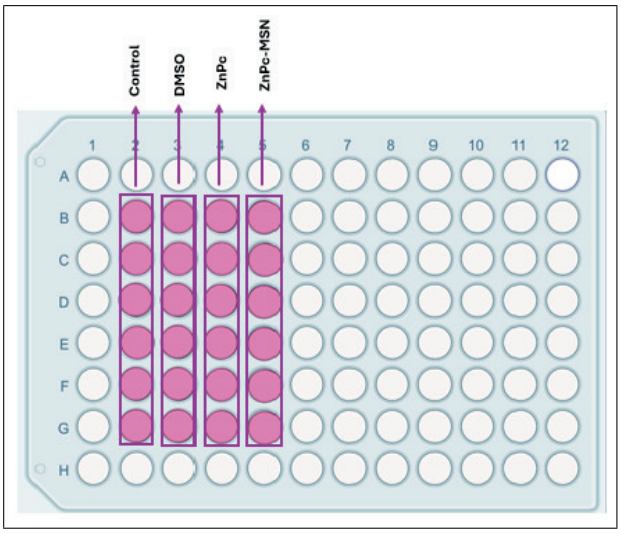


Figure 3.6 Illustration of 96-well plate seeding scheme for comprehensive dark toxicity of ZnPc and ZnPc-MSN.Each group was seeded as six technical replicates.

This experiment plan included control groups, DMSO, ZnPc groups, and ZnPc-MSN groups. After a 24-hour incubation, the cells were treated with 2000 μg/mL ZnPc-MSN and 70.2 μg/mL ZnPc. Following 2 h of incubation, the wells were washed

with PBS,before the additional fresh media, and 24 h later MTT was performed as previously described. Three independent repeats were performed.

3.7 Photodynamic Therapy (PDT) Experiments

Cells were seeded into 96-well plates and divided into five groups: no treatment, light only, dark (no light), 10 minutes, 20 minutes, and 30 minutes of light exposure. After a 24-hour incubation period, 2000 μg/mL of ZnPc-MSN was added to the dark and light groups. Following a 2-hour incubation with ZnPc-MSN, the cells were washed with PBS for three times, and then fresh media were added. The cells were exposed to a 660 nm LED light source (ThorLabs M660L4) with a continuous wavelength (CW) at 100 mW/cm^2 power density except only laser and dark groups. After 24 hours, the MTT process was applied. Three independent replicates were performed.

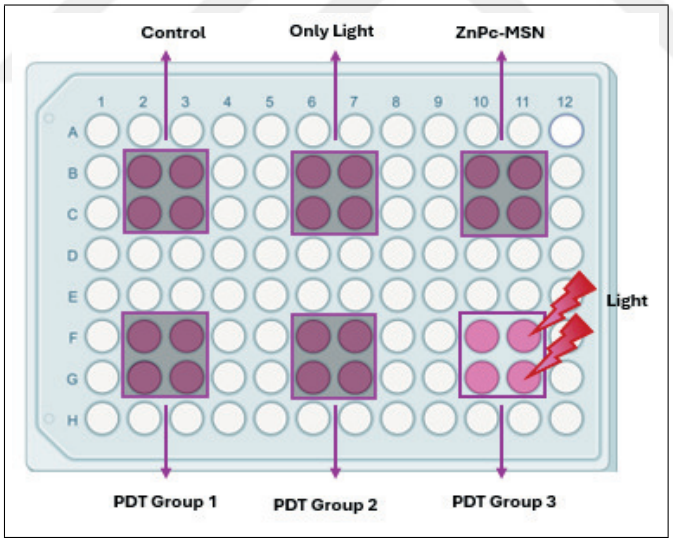


Figure 3.7 Illustration of 96-well plate seeding scheme for PDT experiment, the black cover was always used for groups not currently illuminated. Each group was seeded as four technical replicates.

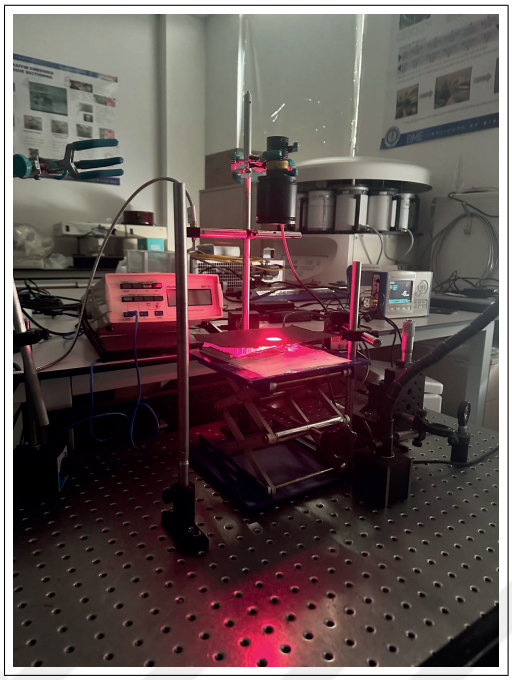


Figure 3.8 PDT experimental setup, with 600 nm LED light source.

3.8 Cellular Uptake Experiment

Cellular uptake of ZnPc and ZnPc-MSN was evaluated based on a previous investigation [61]. Briefly, cells were seeded 10^4 cells in each well and incubated for 24 hours at the 6-well plate.

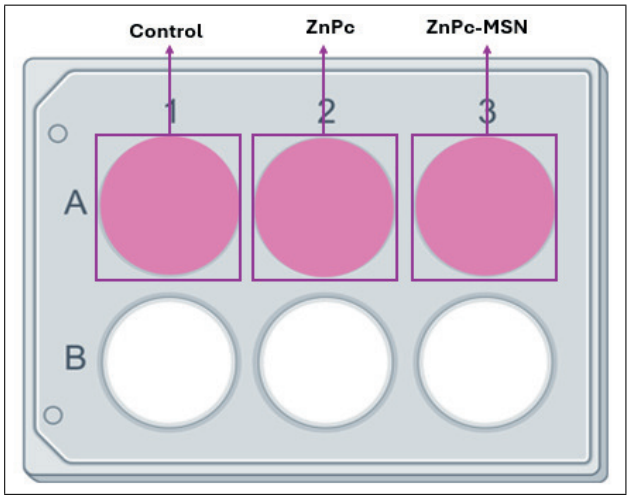


Figure 3.9 Illustration of 6-well plate seeding scheme for cellular uptake experiment.

Subsequently, predetermined concentrations of free ZnPc and ZnPc-MSNs were introduced to the wells and incubated for 2 hours. Following incubation, cells were detached using Tyrpsin-EDTA, transferred into the falcon tubes, and centrifuged at 1000 rpm for 5 minutes. After centrifugation, the cells were gently washed with PBS. Each falcon tube was filled with 500μL of 90% acetone and a distilled water mixture to extract ZnPc from the cells. The supernatants were transferred to a 96-well plate, and a plate reader was used to measure the absorbance at 655 nm. The absorbance values were analyzed using the equation of the standard curve for ZnPc quantification. The equation of standard curve will be referred to as Eq. 3.1.

$$y = 0.0042x + 0.5899 \qquad R^2 = 0.9978 \tag{3.1}$$

where y = *absorbance of supernatants and* x = *concentration of ZnPc.*

To calculate the amount of ZnPc in 1 μl of supernatants the equation of will be referred to as Eq. 3.2.

$$q = x.\frac{M_{ZnPc}}{10^6} \tag{3.2}$$

where q = ZnPc amount in 1 μl of supernatants M_{ZnPc} = molecular weight of ZnPc.

To account for the volume of the solution 500 μl, the absorbance values were multiplied by 500, which is assumed to be constant across all tubes. This correction factor essentially normalizes the absorbance values to a standard volume basis. Finally, the ZnPc uptake per cell was calculated by dividing the corrected absorbance values by the corresponding number of cells in each well. This calculation quantitatively measures the cells free ZnPc and ZnPc-MSN uptake under the experimental conditions.

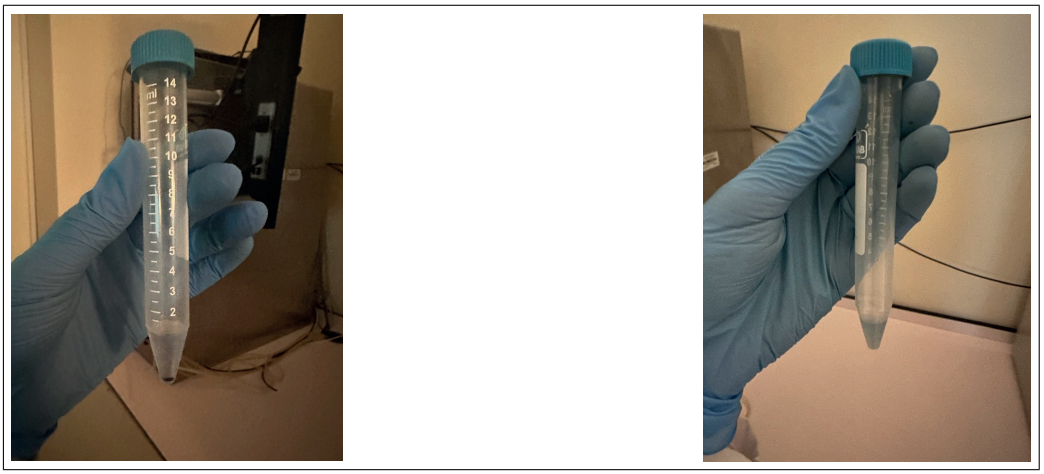


Figure 3.10 Falcon tubes before and after accumulated ZnPc extraction.

3.9 Investigating the Primary PDT Mechanism

The experiment used sodium azide, which quenches singlet oxygen. Therefore, if PDT kills cells via singlet oxygen, adding sodium azide into the media during PDT would inhibit cell death [67].

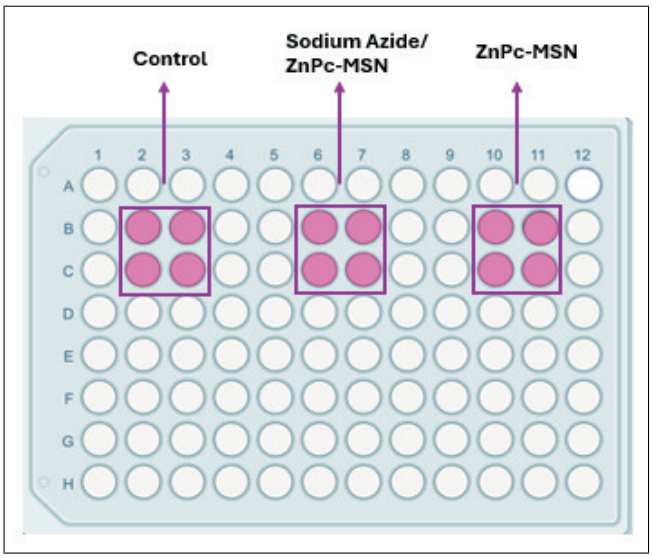


Figure 3.11 Illustration of 96-well plate seeding scheme for investigating the primary PDT mechanism experiment. Each group was seeded as four technical replicates.

First, the nontoxic concentration of sodium azide in A-549 cells was determined. The experimental groups are as follows;

- Control Group

- ZnPc-MSN + sodium azide (50 mM) + light (660 nm 30 minutes 100 mW/cm^2)

- ZnPc-MSN + light (660 nm 30 minutes 100 mW/cm^2)

After 2 hours of incubation, light was applied to the treatment groups. Following 24 hours, MTT was performed. The experiment was repeated two times.

3.10 ROS Production with DPBF Assay

This method evaluates the $^1O_2$ generation capacity of PDT agents. It involves the PDT agents dissolved with a chemical called 1,3-Diphenylisobenzofuran (DPBF) allowed by irradiation with light of a specific wavelength that activates the PDT agents. $^1O_2$ produced during irradiation reacts rapidly with DPBF, leading to a decrease in DPBF's absorbance at 410-420 nm. The extent of this decrease correlates with the amount of $^1O_2$ generated by the PDT agents [68].

The study used ZnPc and ZnPc-MSN at 70.2 μg/mL and 2000 μg/mL with 50 μM DPBF in DMSO, respectively. These were incubated separately with DPBF, and their absorbance at 420 nm was measured after various irradiation times: 0, 5, 10, 15, 20, 25, 30 sec using a UV-Vis spectrophotometer (ThermoScientific/Nanodrop 2000c).

3.11 Photodynamic Stability Experiment

To compare the photostability of ZnPc and ZnPc-MSN, the samples were prepared from previously decided concentrations in transparent falcon tubes and exposed to regular room light. The experiment will involve four exposure time points: 0, 3, 7, and 14 days. Following each period, the peak absorbance values of the sample's UV-Vis spectrophotometer were measured, and the peak absorbance values were compared (ThermoScientific/Nanodrop 2000c). The experiment conducted three different repeats.

3.12 Statistical Analysis

The statistical analysis was performed utilizing a student t-test to compare two independent groups, and the Analysis of Variance (ANOVA) method was used to compare more than two groups after confirming Gaussian distribution; all analyses were conducted on the GraphPrism program. The statistical significance will be accepted as $p<0.05$, indicated as the (**) symbol in the results.

4. RESULTS

4.1 Characterization of Nanoparticles

According to DLS results shown in Figure 4.1, the nanoparticle size is distributed between 80-110 nm [65]. Figures 4.2 indicate that synthesized MSNs exhibits spherical characteristics. The results demonstrate that homogeneous MSNs can be synthesized successfully.

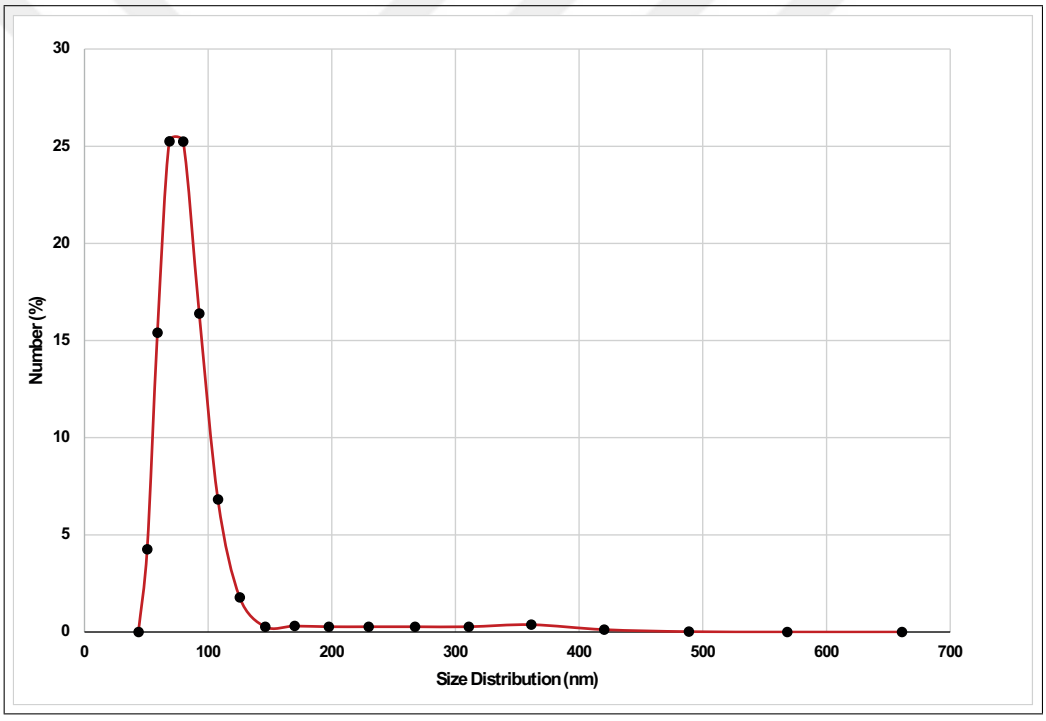


Figure 4.1 DLS Result of MSNs.

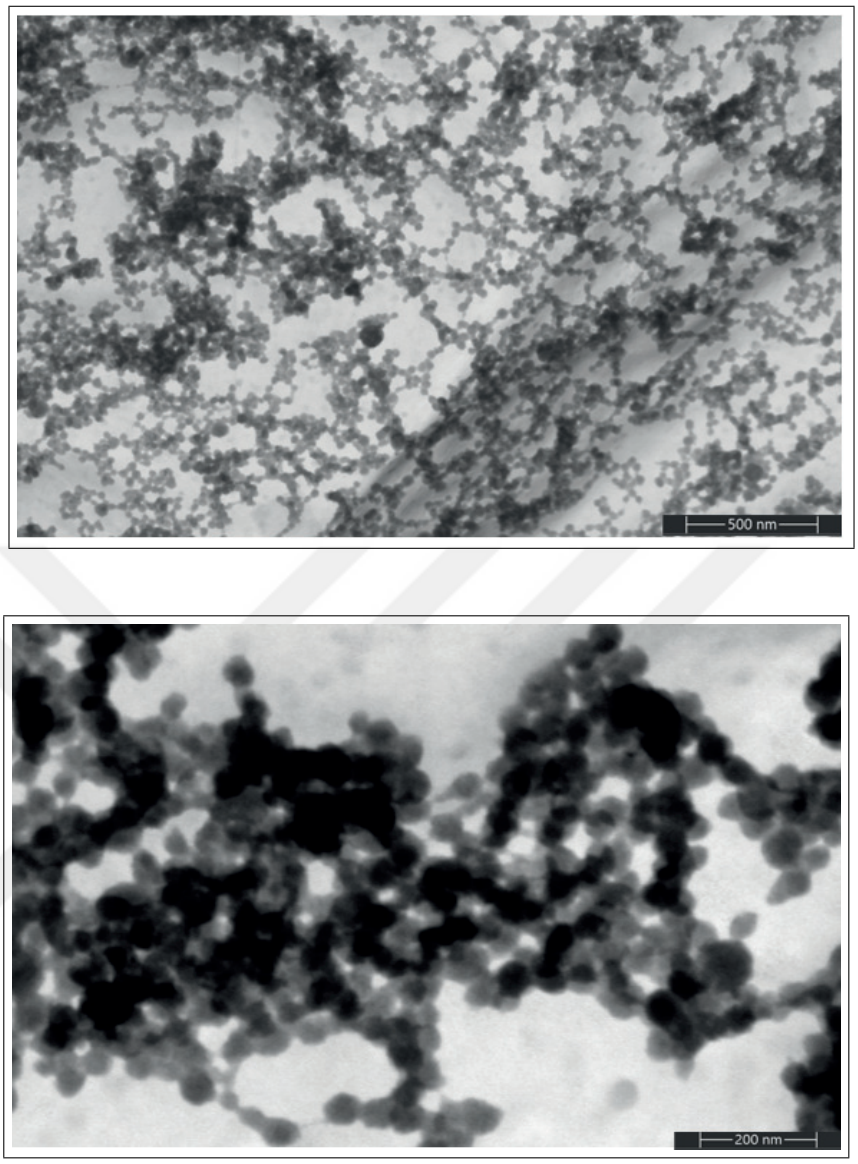


Figure 4.2 MSNs STEM Images demonstrates the physical characterization, scale bars 500 nm, and 200 nm respectively.

4.2 Dark Toxicity Result

According to the dark toxicity results shown in Figure 4.3, ZnPc-MSN does not significantly cytotoxicity in the A-549 cell. For this reason, the highest non-toxic concentration of 2000 μg/mL was determined as the experimental concentration.

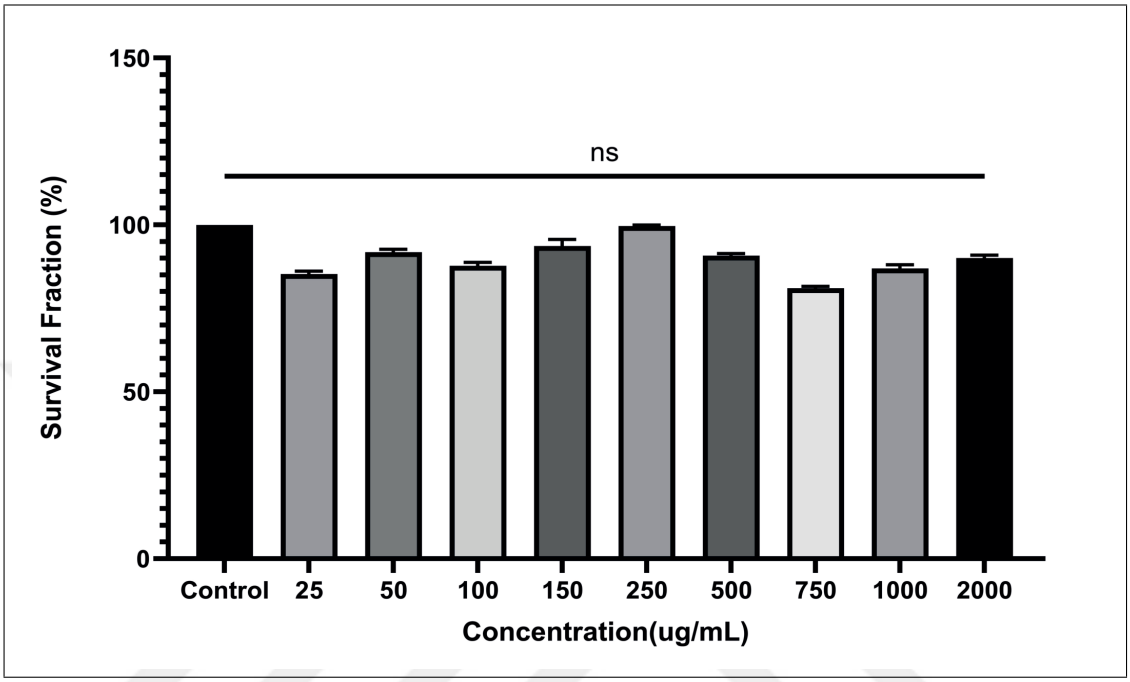


Figure 4.3 Survival fraction result of A-549 cells incubated with different ZnPc-MSN concentration. Data for each group were normalized to the corresponding untreated controls (ns:no significant).

4.3 Determination of loaded amount of ZnPc into the ZnPc-MSN

As in Figure 4.4, the standard curve sketching measures absorbance values of 20-500 μg/mL ZnPc concentration. Based on the standard curve of the linear equation, 2000 μg/mL ZnPc-MSN nanoparticles include 70.2 μg/mL ZnPc.

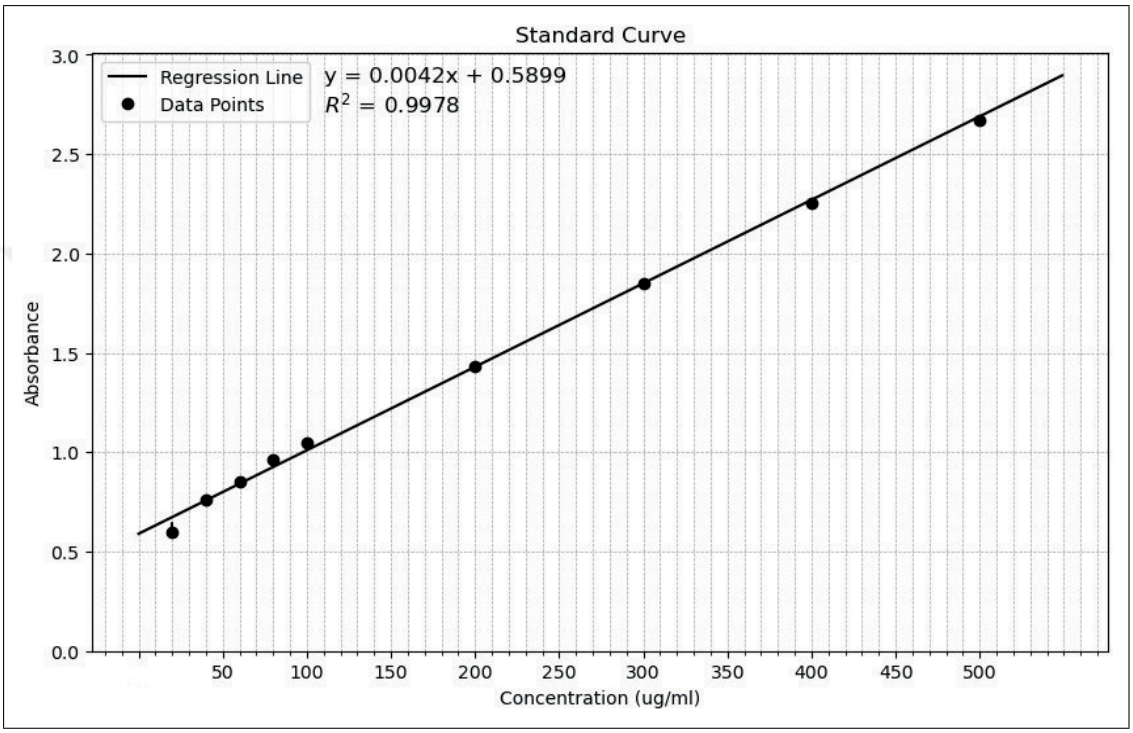


Figure 4.4 Standard curve of ZnPc measuring absorbance values of 20-500 μg/mL.

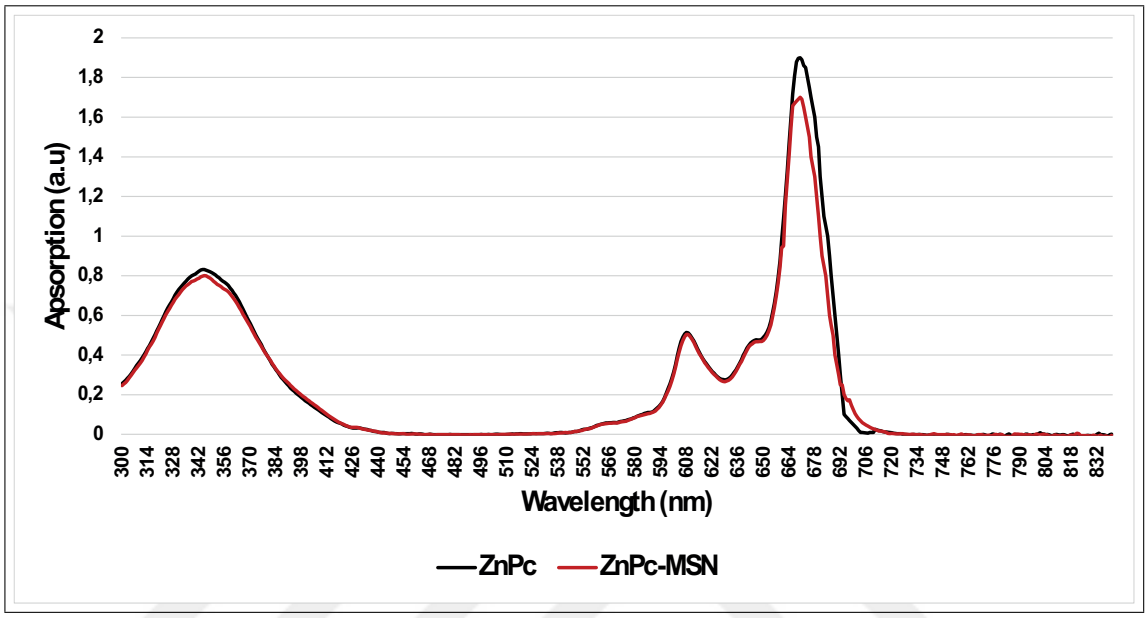


Figure 4.5 Absorbance spectrum of ZnPc (70.2 μg/mL) and ZnPc-MSN (2000 μg/mL).

Figure 4.5 shows the absorption spectrum of ZnPc 70.2 μg/mL and ZnPc-MSN 2000 μg/mL. The similar absorbance values indicate that the ZnPc concentration in ZnPc-MSN was near 70 μg/mL. Additionally, the dark toxicity of free ZnPc and ZnPc-MSN is compared. Figure 4.6 indicates that there are no significant differences between each group. ZnPc was dissolved in DMSO, which is known to be toxic to living cells at high concentrations, so DMSO was added at the same concentration as the experimental group for cytotoxicity analysis.

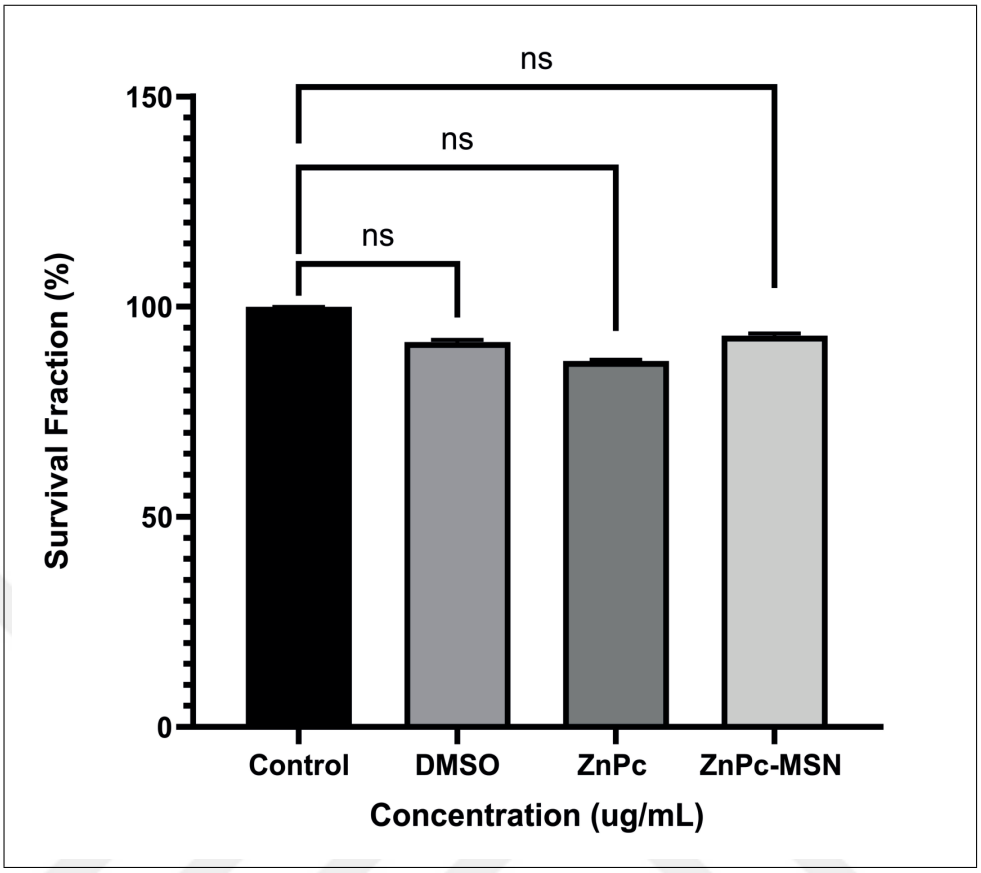


Figure 4.6 Dark toxicity survival fraction of A549 cells treated with ZnPc (70.2 μg/mL) and ZnPc-MSN (2000 μg/mL). Data for each group were normalized to the corresponding untreated controls (ns:no significant).

4.4 Cellular Uptake

Fig 4.7 shows that ZnPc-MSN nanoparticles significantly increase the cellular uptake of the A549 cell compared to ZnPc.

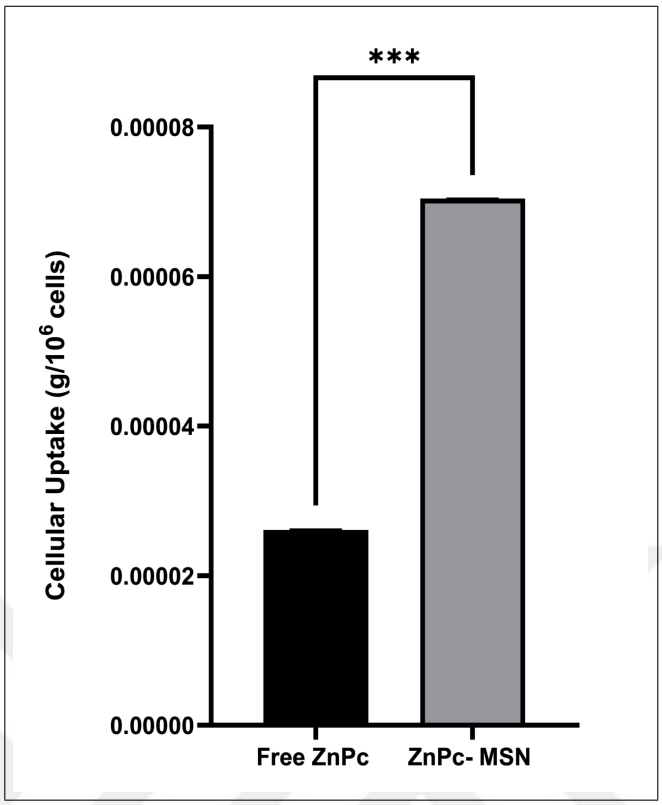


Figure 4.7 Cellular uptake results of ZnPc and ZnPc-MSN.Significant difference marked by (***) (p =0.0007).

4.5 PDT Experiment Result

Figure 4.8 shows that cell irradiation with 660 nm wavelength light and ZnPc-MSN interaction leading substantial cell death in A549 cells compared to control and only light groups. The most effective significant decrease is 180 J/cm^2 (100 mW/cm^2, 30 minutes) of light exposure.

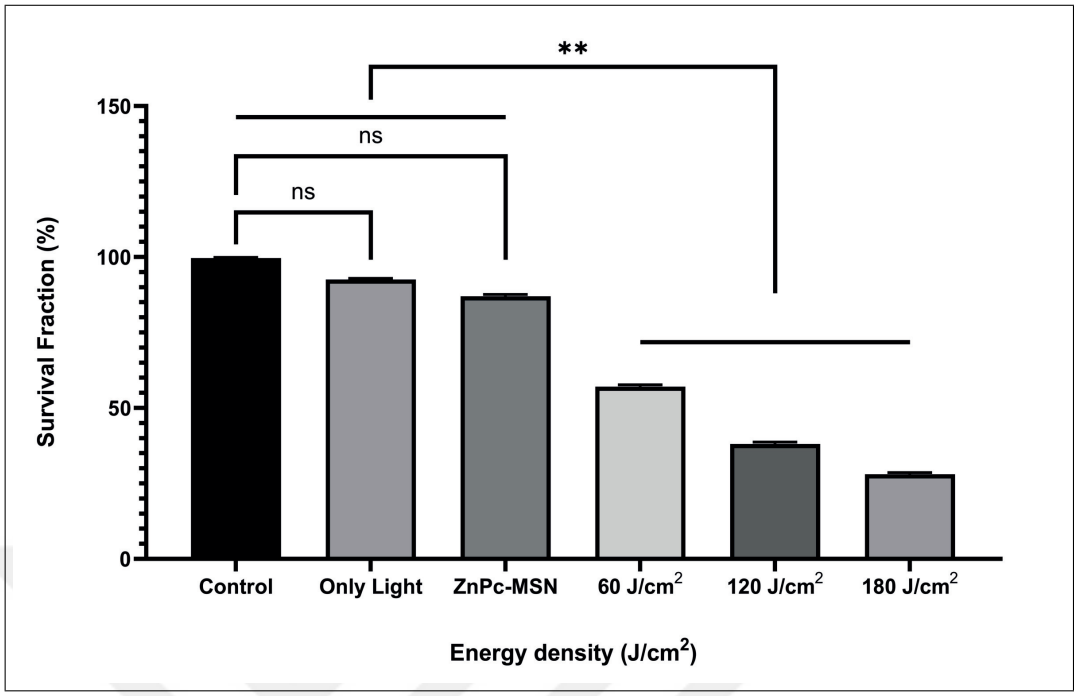


Figure 4.8 Survival Fraction of A549 incubated with ZnPc-MSN and light, only light and only ZnPc-MSN, light irradiation performed with 100 mW/cm^2 and at 660 nm. Data for each group were normalized to the corresponding untreated controls. Significant difference marked by (**) ($p < 0.05$).

4.6 Primary Singlet Oxygen Generation Mechanism

Figure 4.9 indicates that 50 mM sodium azide does not demonstrate a significant cytotoxic effect on A549 cells. Figure 4.10 shows that the with sodium azide and light group significantly pressure the cell death compared to the without sodium azide, which exhibits that the primary mechanism of ZnPc-MSN is $^1O_2$ oxygen production.

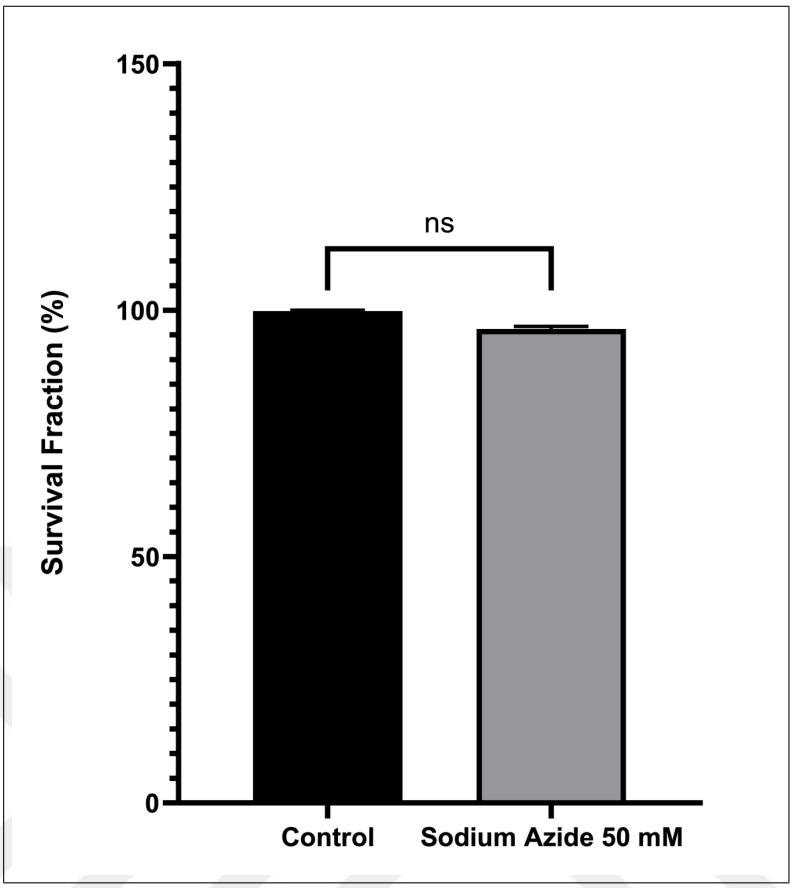


Figure 4.9 Dark toxicity survival fraction of 50 mM Sodium Azide in A-549 cells.Data for the group were normalized to untreated control(ns:no significant).

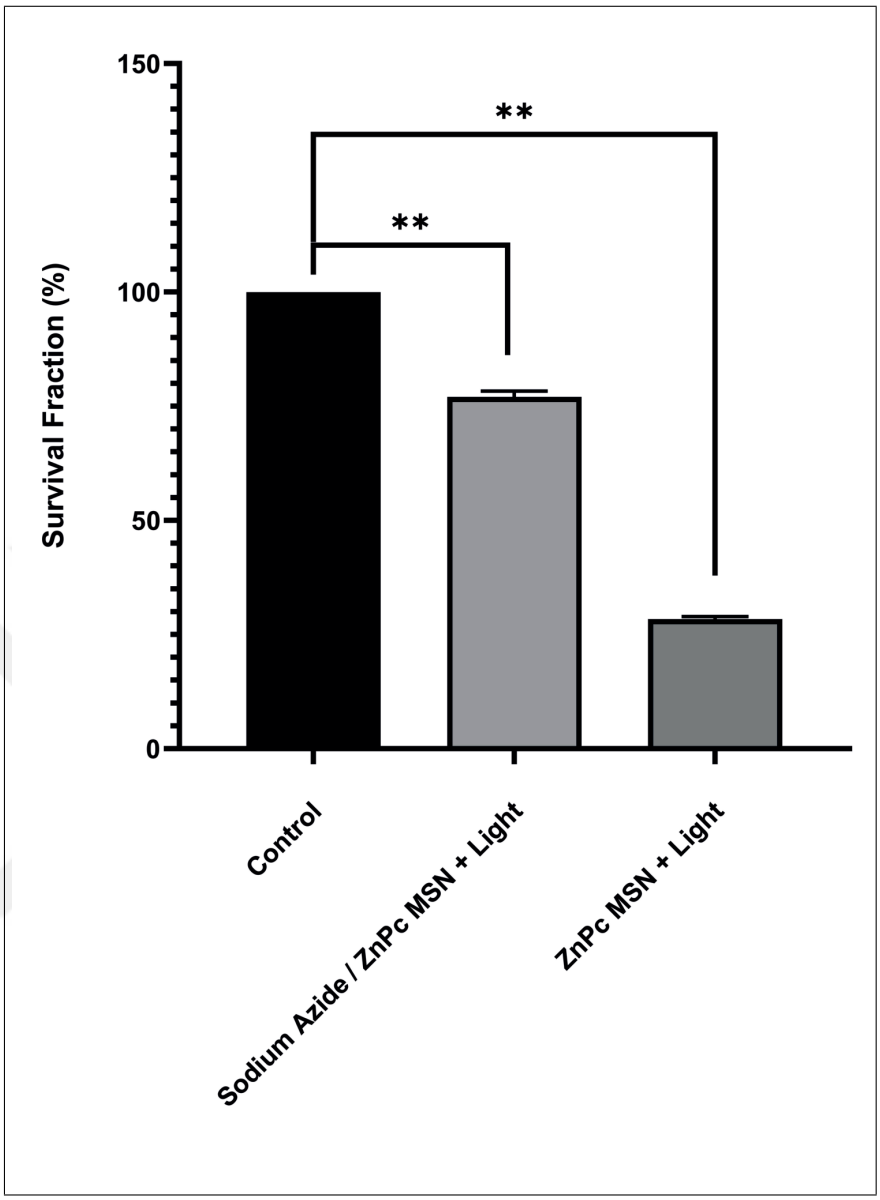


Figure 4.10 Survival fraction of A-549 cells after incubation with and without sodium azide, light irradiation performed with 100 mW/cm^2 and at 660 nm. Data for each group were normalized to the corresponding untreated controls.Significant difference marked by (**) ($p < 0.05$).

4.7 ROS Production DPBF Experiment Result

Fig 4.11 indicates that the presence of ZnPc-MSN leads to absorbance decreases within 5 sec of DPBF at 420 nm, which demonstrates the high $^1O_2$ generation capacity of ZnPc-MSN, and free ZnPc reached the same absorbance at 10 sec.

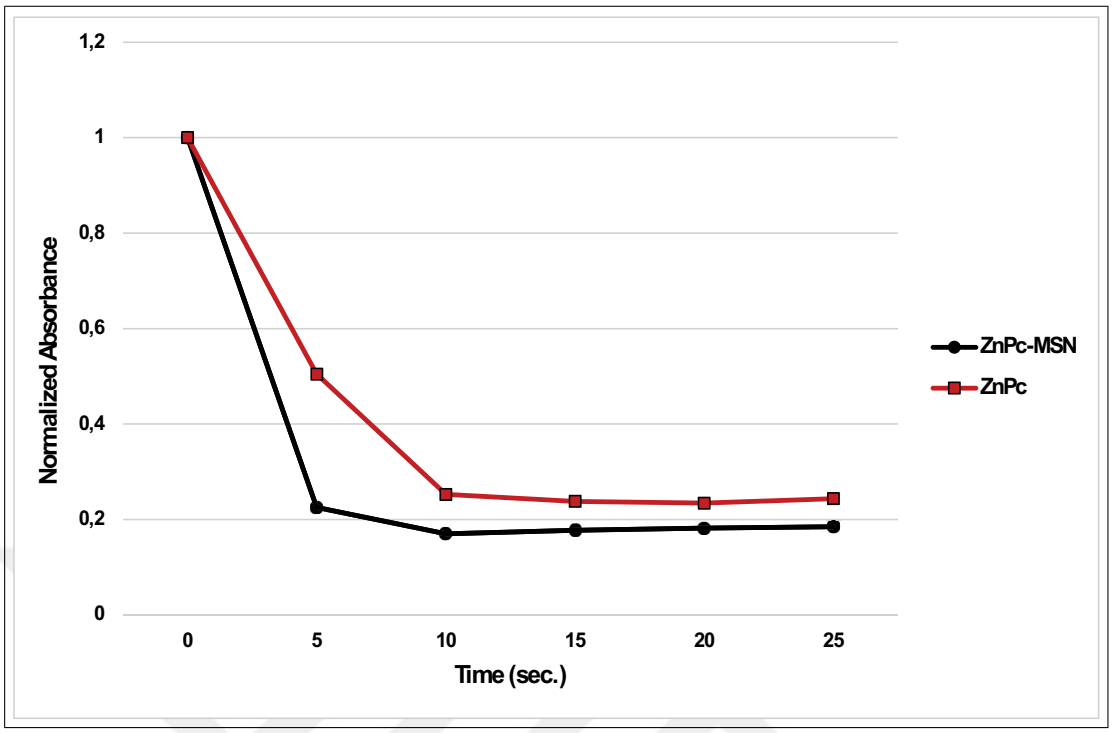


Figure 4.11 ZnPc 70.2 μg/mL and ZnPc-MSN 2000 μg/mL with 50 μ/M DPBF in DMSO absorbance change at 420 nm wavelength.

4.8 Stability Experiment Result

Figures 4.12 and 4.13 show that ZnPc and ZnPc-MSN had adequate photostability at 660 nm when exposed to room light for 14 days.

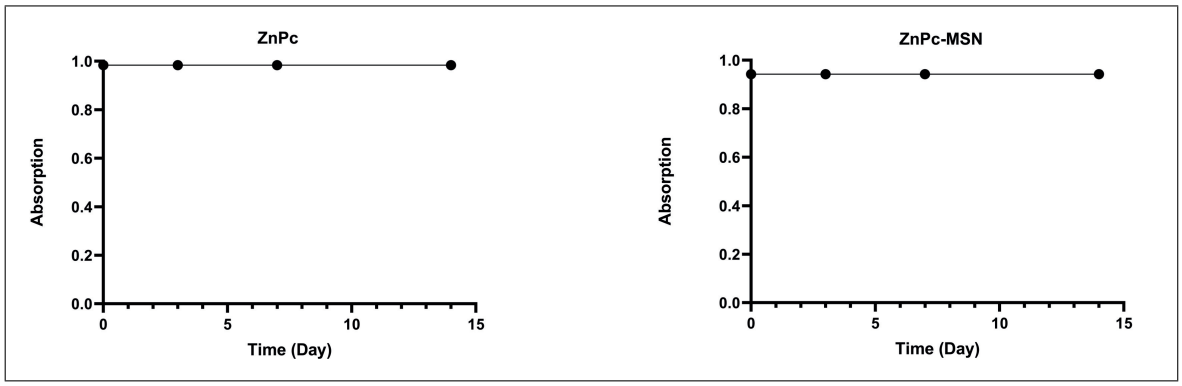


Figure 4.12 Photostability of ZnPc and ZnPc-MSN during 14 days, absorbance at 660 nm.

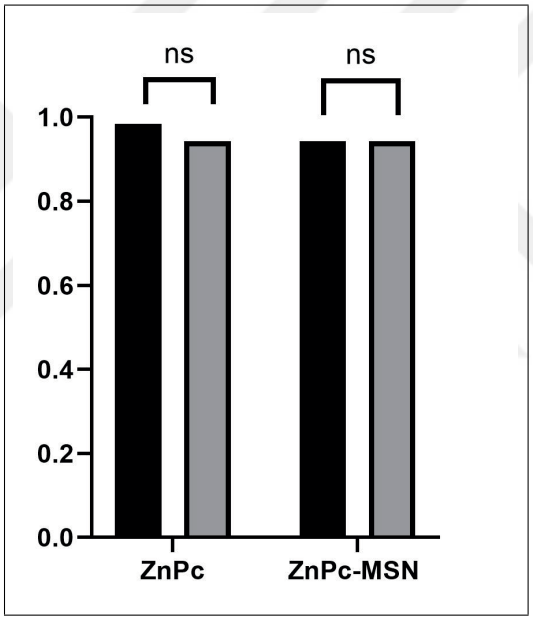


Figure 4.13 Photostability comparison of ZnPc and ZnPc-MSN for at 0 and 14 days, absorbance at 660nm.

5. DISCUSSIONS

ZnPc is a promising PDT agent thanks to its high quantum yield (0.67), biocompatibility, and high absorbance at wavelengths that enable relatively deep tissue penetration [51],[69]. However, the low solubility of ZnPc in aqueous solutions restricts its usage in clinics. To overcome this problem, research continues to assess the modification and/or incorporation of ZnPc with drug delivery systems. The primary goal of this study was to investigate the PDT efficacy of ZnPc-MSN. To do this, we first characterized the synthesized nanoconjugates and then analyzed them in terms of dark toxicity, primary cell killing mechanism, cellular uptake, $^1O_2$ generation, PDT efficacy and photostability. The ZnPc concentration in 2000 μg/mL MSNs was calculated as 70.2 μg/mL using a standard curve. Material characterization was performed using STEM imaging and DLS measuring techniques, which revealed that the nanoparticles were spherical and distributed between 80-110 nm [65].

The FDA acknowledges silica as safe and it is commonly used as a supplement or an ingredient in medications [58]. Additionally, thanks to their large pore capacity, MSNs can enhance the delivery of hydrophobic cargo in the bloodstream and protect it from enzymatic degradation [7],[59]. The results of our dark toxicity experiments revealed that ZnPc-MSN did not cause any toxicity on A-549 cells up to 2000 μg/mL concentration, which is in accordance with the literature [69]. As Tu et al. and Liu et al. observed, in our PDT experiments using 660 nm led light source at 100 mW/cm^2, we saw a statistically significant decrease in the survival fraction when the cells were irradiated with energy densities 60 J/cm^2, 120 J/cm^2, and 180 J/cm^2 [6],[61].

Sodium azide, which is a singlet oxygen quencher, can be used to determine the primary mechanism PDT-mediated cell death [67]. In our study, we observed that the presence of sodium azide significantly inhibited the efficacy of PDT, which revealed that $^1O_2$ produced by Type II reactions was primarily responsible for cell killing (Figure 4.10). On the other hand, it can be said the Type I mechanism contributes to ROS

production because the presence of sodium azide did not completely inhibit cell killing. The DPBF assay was conducted to compare the $^1O_2$ generation of free and MSN-incorporated ZnPc. Figure 4.11 shows the decrease in absorbance of DPBF at 420 nm was within 5 second for ZnPc-MSN, however, it took within 10 seconds for free ZnPc. In a similar study, Depra et al. showed that ZnPc incorporated with chitosan nanoparticles demonstrated high ROS production ability compared to free ZnPc [70]. In this experiment, we also observed that the absorbance of DPBF at 420 nm did not decrease to zero no matter how long the samples were irradiated, which was not due to incomplete DPBF degradation but because ZnPc has minor absorbance at that wavelength.

According to the results of cellular uptake experiments, the cellular uptake of ZnPc-MSN was significantly higher than free ZnPc ($p<0.0007$). This result may stem from the hydrophobic nature of ZnPc, which restricts its cellular uptake. Also, the surface modification of MSN might enable improved cellular uptake and increased endosomal escape efficacy [6],[71].

The photostability experiment shows that both free ZnPc and ZnPc-MSN are highly photostable under room light. The stability of the Pcs structure is contingent upon the electron distribution within its conjugated bonding system. An even distribution of π-electrons across this system reinforces the Pcs moiety. Moreover, employing electron-withdrawing solvents like DMSO can potentially augment the molecular resilience of Pcs subjected to UV excitation [72]. Additionally, Depra et al. investigated photostability at UV-Vis absorption, showing that free ZnPc and ZnPc-loaded nanoparticle systems have appropriate photostability in PDT usage [70].

While the results from this study are encouraging, the evaluation of ZnPc-MSN's therapeutic potential was confined to a single cancer cell line. A broader investigation, encompassing a diverse range of cancer cell lines, must assess its applicability in PDT. Subsequent research will examine the surface modification of MSN to increase cellular uptake and augment the endosomal escape efficacy of in vivo experiments. Additionally, co-PS loading might be evaluated to increase the PDT effect.

6. CONCLUSION

This study investigated the photodynamic therapeutic potential of the ZnPc-MSN nanoparticle system in the A-549 lung cancer cell line. Successful synthesis and characterization of ZnPc-MSN nanoparticles showed that integrating ZnPc into MSN was advantageous because it allowed water solubility.

The obtained ZnPc-MSN exhibited favorable cellular uptake, high light-induced ROS production, and low dark cytotoxicity, demonstrating their potential as an effective PS.

In conclusion, this research provides a basic framework for future studies to evaluate the biodistribution, pharmacokinetics, and toxicity profile of ZnPc-MSN in vivo studies to optimize surface modification of nanoparticle parameters for improved therapeutic outcomes. Further research is required to analyze its efficacy in various cancer types comprehensively. Dual PS loading and combined treatments such as chemotherapies and PDT or PTT can be evaluated to improve clinical outcomes.

REFERENCES

1. Siegel, R. L., A. N. Giaquinto, and A. Jemal, "Cancer statistics, 2024.," *CA: ACancer Journal For Clinicians*, Vol. 74, no. 1, 2024.

2. dos Santos, A. F., D. Q. de Almeida, L. F. Terra, M. S. Baptista, and L. Labriola, "Photodynamic therapy in cancer treatment-an update review," *J.Cancer Metastasis Treat*, Vol. 5, no. 25, pp. 10–20517, 2019.

3. Greish, K., "Enhanced permeability and retention (epr) effect for anticancer nanomedicine drug targeting," *Cancer Nanotechnology: Methods and Protocols*, pp. 25–37, 2010.

4. Castano, A. P., T. N. Demidova, and M. R. Hamblin, "Mechanisms in photodynamic therapy: Part one—photosensitizers, photochemistry and cellular localization," *Photodiagnosis and Photodynamic Therapy*, Vol. 1, no. 4, pp. 279–293, 2004.

5. Lu, J., M. Liong, J. I. Zink, and F. Tamanoi, "Mesoporous silica nanoparticles as a delivery system for hydrophobic anticancer drugs," *Small*, Vol. 3, no. 8, pp. 1341–1346, 2007.

6. Tu, J., T. Wang, W. Shi, G. Wu, X. Tian, Y. Wang, D. Ge, and L. Ren, "Multifunctional znpc-loaded mesoporous silica nanoparticles for enhancement of photodynamic therapy rfficacy by endolysosomal escape," *Biomaterials*, Vol. 33, no. 31, pp. 7903–7914, 2012.

7. Li, Z., J. C. Barnes, A. Bosoy, J. F. Stoddart, and J. I. Zink, "Mesoporous silica nanoparticles in biomedical applications," *Chemical Society Reviews*, Vol. 41, no. 7, pp. 2590–2605, 2012.

8. Roguin, L. P., N. Chiarante, M. C. G. Vior, and J. Marino, "Zinc (ii) phthalocyanines as photosensitizers for antitumor photodynamic therapy," *The International jJournal of Biochemistry & Cell Biology*, Vol. 114, p. 105575, 2019.

9. Amin, C. S., A. F. El Essawy, R. A. Elhefny, R. Y. Abu El-Ela, and E. S. Farhat, "Outcomes of suspected thoracic malignancy patients with initial non diagnostic bronchoscopy," *Fayoum University Medical Journal*, Vol. 13, no. 3, pp. 11–27, 2024.

10. Travis, W. D., "Pathology of lungcancer," *Clinics in Chest Medicine*, Vol. 32, no. 4, pp. 669–692, 2011.

11. UK, C. R., "Cancer reserach uk available: https://www.cancerresearchuk.org/," 2022.

12. WHO, "World health organization available: www.who.int," 2023.

13. Kreisman, H., N. Wolkove, and E. Quoix, "Small cell lungcancer presenting as a solitary pulmonary nodule," *Chest*, Vol. 101, no. 1, pp. 225–231, 1992.

14. Krug, L., M. Kris, K. Rosenzweig, and W. Travis, "Small cell and other neuroendocrine tumors of the lung," *Cancer: Principles & Practice of Oncology*, Vol. 1, pp. 946–971, 2008.

15. Myers, D. J., and J. M. Wallen, "Lung adenocarcinoma," in *StatPearls [Internet]*, StatPearls Publishing, 2023.

16. Sabbula, B. R., D. P. Gasalberti, and F. Anjum, "Squamous cell lungcancer," in *StatPearls*, StatPearls Publishing, 2023.

17. Gadgeel, S. M., S. S. Ramalingam, and G. P. Kalemkerian, "Treatment of lungcancer," *Radiologic Clinics*, Vol. 50, no. 5, pp. 961–974, 2012.

18. Govindan, R., N. Page, D. Morgensztern, W. Read, R. Tierney, A. Vlahiotis, E. L. Spitznagel, and J. Piccirillo, "Changing epidemiology of small-cell lungcancer in the united states over the last 30 years: Analysis of the surveillance, epidemiologic, and end results database," *Journal of Clinical Oncology*, Vol. 24, no. 28, pp. 4539–4544, 2006.

19. "Cancer reserach uk available: https://www.cancerresearchuk.org/about-cancer/lung-cancer/stages-types-grades/limited-extensive."

20. Rudin, C. M., E. Brambilla, C. Faivre-Finn, and J. Sage, "Small-cell lungcancer," *Nature Reviews Disease Primers*, Vol. 7, no. 1, p. 3, 2021.

21. Hii, A. R. K., X. Qi, and Z. Wu, "Advanced strategies for crispr/cas9 delivery and applications in gene editing, therapy, and cancer detection using nanoparticles and nanocarriers," *Journal of Materials Chemistry B*, Vol. 12, no. 6, pp. 1467–1489, 2024.

22. Mitin, T., A. Jain, C. Degnin, Y. Chen, M. Henderson, and C. R. Thomas Jr, "Current patterns of care for patients with extensive stage small cell lungcancer: Survey of us radiation oncologists on their recommendations regarding thoracic consolidation radio therapy," *Lungcancer*, Vol. 100, pp. 85–89, 2016.

23. Horn, L., A. S. Mansfield, A. Szczęsna, L. Havel, M. Krzakowski, M. J. Hochmair, F. Huemer, G. Losonczy, M. L. Johnson, M. Nishio, and Others, "First-line atezolizumab plus chemotherapy in extensive-stage small-cell lungcancer," *New England Journal of Medicine*, Vol. 379, no. 23, pp. 2220–2229, 2018.

24. Rudin, C. M., M. M. Awad, A. Navarro, M. Gottfried, S. Peters, T. Csőszi, P. K. Cheema, D. Rodriguez-Abreu, M. Wollner, J. C.-H. Yang, and Others, "Pembrolizumab or placebo plus etoposide and platinum as first-line therapy for extensive-stage small-cell lungcancer: Randomized, double-blind, phase iii keynote-604 study," *Journal of Clinical Oncology*, Vol. 38, no. 21, pp. 2369–2379, 2020.

25. Wang, K., Y. Zhang, J. Wang, A. Yuan, M. Sun, J. Wu, and Y. Hu, "Self-assembled ir780-loaded transferrin nanoparticles as an imaging, targeting and pdt/ptt agent for cancer therapy," *Scientific Reports*, Vol. 6, no. 1, p. 27421, 2016.

26. Saneja, A., R. Kumar, D. Arora, S. Kumar, A. K. Panda, and S. Jaglan, "Recent advances in near-infrared light-responsive nanocarriers for cancer therapy," *Drug Discovery Today*, Vol. 23, no. 5, pp. 1115–1125, 2018.

27. Dolmans, D. E., D. Fukumura, and R. K. Jain, "Photodynamic therapy for cancer," *Nature ReviewsCancer*, Vol. 3, no. 5, pp. 380–387, 2003.

28. Kwiatkowski, S., B. Knap, D. Przystupski, J. Saczko, E. Kędzierska, K. Knap-Czop, J. Kotlińska, O. Michel, K. Kotowski, and J. Kulbacka, "Photodynamic therapy-mechanisms, photosensitizers and combinations," *Biomedicine & PharmacOtherapy*, Vol. 106, pp. 1098–1107, 2018.

29. Robertson, C. A., D. H. Evans, and H. Abrahamse, "Photodynamic therapy (pdt): A short review on cellular mechanisms and cancer research applications for pdt," *Journal of Photochemistry and Photobiology B: Biology*, Vol. 96, no. 1, pp. 1–8, 2009.

30. Luksiene, Z., "Photodynamic therapy: Mechanism of action and ways to improve the efficiency of treatment," *Medicina (Kaunas, Lithuania)*, Vol. 39, no. 12, pp. 1137–1150, 2003.

31. Chin, Y., S. H. Lim, Y. Zorlu, V. Ahsen, L. V. Kiew, L. Y. Chung, F. Dumoulin, and H. B. Lee, "Improved photodynamic efficacy of zn (ii) phthalocyanines via glycerol substitution," *PloS One*, Vol. 9, no. 5, p. e97894, 2014.

32. Kessel, D., and N. L. Oleinick, "Photodynamic therapy and cell death pathways," *Photodynamic Therapy: Methods and Protocols*, pp. 35–46, 2010.

33. Plaetzer, K., T. Kiesslich, T. Verwanger, and B. Krammer, "The modes of cell death induced by pdt: An overview," *Medical Laser Application*, Vol. 18, no. 1, pp. 7–19, 2003.

34. Kessel, D., "Photodynamic therapy: From the beginning," *Photodiagnosis and Photodynamic Therapy*, Vol. 1, no. 1, pp. 3–7, 2004.

35. Agostinis, P., K. Berg, K. A. Cengel, T. H. Foster, A. W. Girotti, S. O. Gollnick, S. M. Hahn, M. R. Hamblin, A. Juzeniene, D. Kessel, and Others, "Photodynamic therapy of cancer: An update," *CA: ACancer Journal For Clinicians*, Vol. 61, no. 4, pp. 250–281, 2011.

36. Bonnett, R., *Chemical Aspects of Photodynamic Therapy*, CRC Press, 2000.

37. Ömeroğlu, İ., and M. Durmuş, "Water-soluble phthalocyanine photosensitizers for photodynamic therapy," *Turkish Journal of Chemistry*, Vol. 47, no. 5, pp. 837–863, 2023.

38. Machacek, M., A. Cidlina, V. Novakova, J. Svec, E. Rudolf, M. Miletin, R. Kucera, T. Simunek, and P. Zimcik, "Far-red-absorbing cationic phthalocyanine photosensitizers: Synthesis and evaluation of the ahotodynamic anticancer activity and the mode of cell death induction," *Journal of Medicinal Chemistry*, Vol. 58, no. 4, pp. 1736–1749, 2015.

39. Ion, R.-M., "The use of phthalocyanines and related complexes in photodynamic therapy," in *Photosensitizers in Medicine, Environment, and Security*, pp. 315–349, Springer, 2011.

40. Abrahamse, H., and M. R. Hamblin, "New photosensitizers for photodynamic therapy," *Biochemical Journal*, Vol. 473, no. 4, pp. 347–364, 2016.

41. Lucky, S. S., K. C. Soo, and Y. Zhang, "Nanoparticles in photodynamic therapy," *Chemical Reviews*, Vol. 115, no. 4, pp. 1990–2042, 2015.

42. Calixto, G. M. F., J. Bernegossi, L. M. De Freitas, C. R. Fontana, and M. Chorilli, "Nanotechnology-based drug delivery systems for photodynamic therapy of cancer: A review," *Molecules*, Vol. 21, no. 3, p. 342, 2016.

43. Jawahar, N., and S. Meyyanathan, "Polymeric nanoparticles for drug delivery and targeting: A comprehensive review," *International Journal of Health & Allied Sciences*, Vol. 1, no. 4, pp. 217–217, 2012.

44. Ortiz, R., L. Cabeza, M. C. Leiva, J. Jimenez-Lopez, C. Melguizo, and J. Prados, "Nanomedical platform for drug delivery in cancer," *Current Organic Chemistry*, Vol. 21, no. 23, pp. 2376–2399, 2017.

45. Deng, S., M. R. Gigliobianco, R. Censi, and P. Di Martino, "Polymeric nanocapsules as nanotechnological alternative for drug delivery system: Current status, challenges and opportunities," *Nanomaterials*, Vol. 10, no. 5, p. 847, 2020.

46. Lee, D., S. Kwon, S.-y. Jang, E. Park, Y. Lee, and H. Koo, "Overcoming the obstacles of current photodynamic therapy in tumors using nanoparticles," *Bioactive Materials*, Vol. 8, pp. 20–34, 2022.

47. Fang, J., H. Nakamura, and H. Maeda, "The epr effect: Unique features of tumor blood vessels for drug delivery, factors involved, and limitations and augmentation of the effect," *Advanced Drug Delivery Reviews*, Vol. 63, no. 3, pp. 136–151, 2011.

48. Sorrin, A. J., M. Kemal Ruhi, N. A. Ferlic, V. Karimnia, W. J. Polacheck, J. P. Celli, H.-C. Huang, and I. Rizvi, "Photodynamic therapy and the biophysics of the tumor microenvironment," *Photochemistry and Photobiology*, Vol. 96, no. 2, pp. 232–259, 2020.

49. Santos, K. L. M., R. M. Barros, D. P. da Silva Lima, A. M. A. Nunes, M. R. Sato, R. Faccio, B. P. G. de Lima Damasceno, and J. A. Oshiro-Junior, "Prospective application of phthalocyanines in the photodynamic therapy against microorganisms and tumor cells: A mini-review," *Photodiagnosis and Photodynamic Therapy*, Vol. 32, p. 102032, 2020.

50. Gao, J., Z. Chen, X. Li, M. Yang, J. Lv, H. Li, and Z. Yuan, "Chemiluminescence in combination with organic photosensitizers: Beyond the light penetration depth limit of photodynamic therapy," *International Journal of Molecular Sciences*, Vol. 23, no. 20, p. 12556, 2022.

51. Ogunsipe, A., D. Maree, and T. Nyokong, "Solvent effects on the photochemical and fluorescence properties of zinc phthalocyanine derivatives," *Journal of Molecular Structure*, Vol. 650, no. 1-3, pp. 131–140, 2003.

52. Plaetzer, K., B. Krammer, J. Berlanda, F. Berr, and T. Kiesslich, "Photophysics and photochemistry of photodynamic therapy: Fundamental aspects," *Lasers in Medical Science*, Vol. 24, pp. 259–268, 2009.

53. Prasad, P. N., *Introduction to Biophotonics*, John Wiley & Sons, 2004.

54. Velazquez, F. N., M. Miretti, M. T. Baumgartner, B. L. Caputto, T. C. Tempesti, and C. G. Prucca, "Effectiveness of znpc and of an amine derivative to inactivate glioblastoma cells by photodynamic therapy: an in vitro comparative study," *Scientific Reports*, Vol. 9, no. 1, p. 3010, 2019.

55. Soriano, J., A. Villanueva, J. C. Stockert, and M. Cañete, "Vehiculization determines the endocytic internalization mechanism of zn (ii)-phthalocyanine," *Histochemistry and Cell Biology*, Vol. 139, pp. 149–160, 2013.

56. Chen, D., M. Song, J. Huang, N. Chen, J. Xue, and M. Huang, "Photocyanine: A novel and effective phthalocyanine-based photosensitizer for cancer treatment," *Journal of Innovative Optical Health Sciences*, Vol. 13, no. 03, p. 2030009, 2020.

57. Medicine, N. L., "Nih library of medicine available: https://clinicaltrials.gov/," 2010.

58. Gisbert-Garzarán, M., and M. Vallet-Regí, "Influence of the surface functionalization on the fate and performance of mesoporous silica nanoparticles," *Nanomaterials*, Vol. 10, no. 5, p. 916, 2020.

59. Manzano, M., and M. Vallet-Regí, "Mesoporous silica nanoparticles for drug delivery," *Advanced Functional Materials*, Vol. 30, no. 2, p. 1902634, 2020.

60. Lin, A.-L., S.-Z. Li, C.-H. Xu, X.-S. Li, B.-Y. Zheng, J.-J. Gu, M.-R. Ke, and J.-D. Huang, "A ph-responsive stellate mesoporous silica based nanophotosensitizer for in vivo-cancer diagnosis and targeted photodynamic therapy," *Biomaterials Science*, Vol. 7, no. 1, pp. 211–219, 2019.

61. Liu, W., Y. Tian, Y. Zhang, K. Liu, S. Zhao, J. Zhang, Y. Su, Y. Zhao, Y. Tang, J. Sun, and Others, "Timely coordinated phototherapy mediated by mesoporous organosilica coated triangular gold nanoprisms," *Journal of Materials Chemistry B*, Vol. 6, no. 23, pp. 3865–3875, 2018.

62. Ma, J., H. Wu, Y. Li, Z. Liu, G. Liu, Y. Guo, Z. Hou, Q. Zhao, D. Chen, and X. Zhu, "Novel core-interlayer-shell dox/znpc co-loaded msns@ ph-sensitive cap@ pegylated liposome for enhanced synergetic chemo-photodynamic therapy," *Pharmaceutical Research*, Vol. 35, pp. 1–12, 2018.

63. Qian, H. S., H. C. Guo, P. C.-L. Ho, R. Mahendran, and Y. Zhang, "Mesoporous-silica-coated up-conversion fluorescent nanoparticles for photodynamic therapy," *Small*, Vol. 5, no. 20, pp. 2285–2290, 2009.

64. Prieto-Montero, R., T. Arbeloa, and V. Martínez-Martínez, "Photosensitizer-mesoporous silica nanoparticles combination for enhanced photodynamic therapy," *Photochemistry and Photobiology*, Vol. 99, no. 3, pp. 882–900, 2023.

65. Lin, Y.-S., and C. L. Haynes, "Impacts of mesoporous silica nanoparticle size, pore ordering, and pore integrity on hemolytic activity," *Journal of The American Chemical Society*, Vol. 132, no. 13, pp. 4834–4842, 2010.

66. Malm, A. V., and J. C. Corbett, "Improved dynamic light scattering using an adaptive and statistically driven time resolved treatment of correlation data," *Scientific Reports*, Vol. 9, no. 1, p. 13519, 2019.

67. Huang, L., T. G. S. Denis, Y. Xuan, Y.-Y. Huang, M. Tanaka, A. Zadlo, T. Sarna, and M. R. Hamblin, "Paradoxical potentiation of methylene blue-mediated antimicrobial photodynamic inactivation by sodium azide: Role of ambient oxygen and azide radicals," *Free Radical Biology and Medicine*, Vol. 53, no. 11, pp. 2062–2071, 2012.

68. Sun, K., Y. Ge, J. Yang, and X. Hu, "Synthesis, photophysical properties and dna-photocleavage activity of silicon phthalocyanine derivatives," *Pharmacology & Pharmacy*, Vol. 13, no. 6, pp. 174–188, 2022.

69. Avci, P., A. Gupta, M. Sadasivam, D. Vecchio, Z. Pam, N. Pam, and M. R. Hamblin, "Low-level laser (light) therapy (lllt) in skin: Stimulating, healing, restoring," in *Seminars in Cutaneous Medicine and Surgery*, Vol. 32, p. 41, NIH Public Access, 2013.

70. De Souza, T. D., F. I. Ziembowicz, D. F. Mueller, S. C. Lauermann, C. L. Kloster, R. C. V. Santos, L. Q. S. Lopes, A. F. Ourique, G. Machado, and M. A. Villetti, "Evaluation of photodynamic activity, photostability and in vitro drug release of zinc phthalocyanine-loaded nanocapsules," *European Journal of Pharmaceutical Sciences*, Vol. 83, pp. 88–98, 2016.

71. Wong, R. C., D. K. Ng, W.-P. Fong, and P.-C. Lo, "Encapsulating ph-responsive doxorubicin-phthalocyanine conjugates in mesoporous silica nanoparticles for combined photodynamic therapy and controlled chemotherapy," *Chemistry-A European Journal*, Vol. 23, no. 65, pp. 16505–16515, 2017.

72. Słota, R., and G. Dyrda, "Uv photostability of metal phthalocyanines in organic solvents," *Inorganic Chemistry*, Vol. 42, no. 18, pp. 5743–5750, 2003.